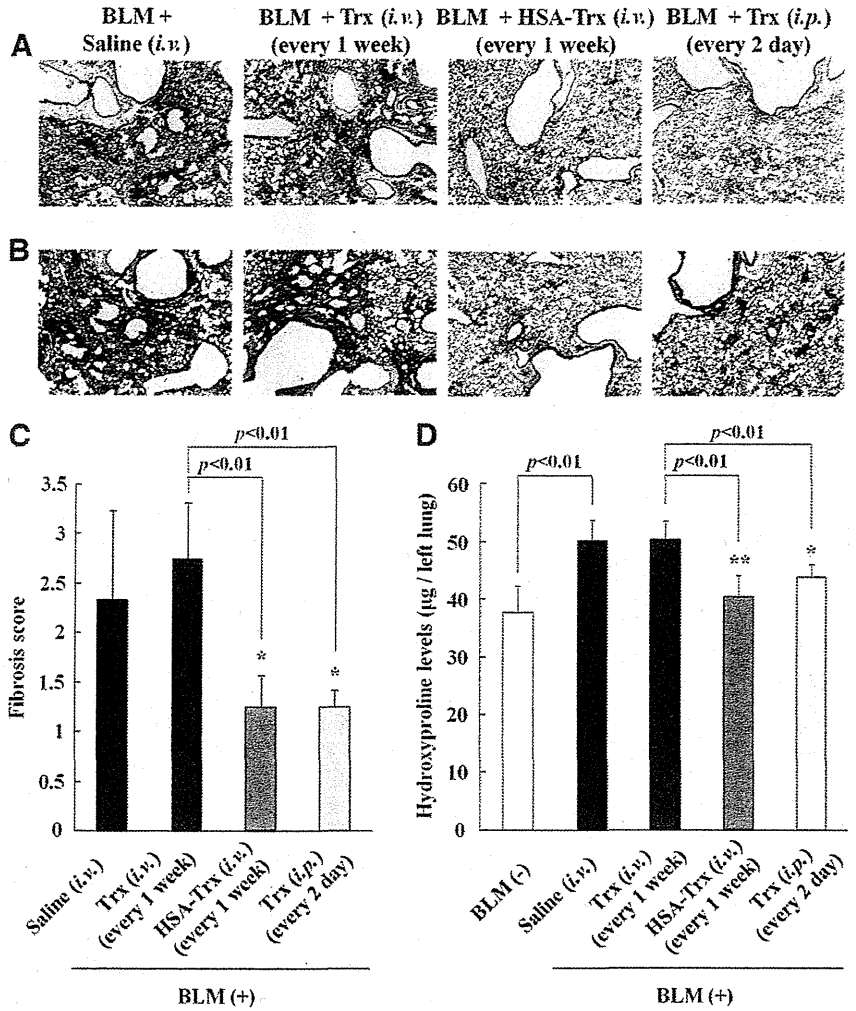

Fig. 3. Effects of HSA-Trx (intravenously; every 1 week), Trx (intravenously; every 1 week), or Trx (intraperitoneally; every 2 days) on the BLM-induced pulmonary fibrosis. (A and B) Sections of pulmonary tissue were prepared 14 days after BLM administration and subjected to histopathological examination ([A] H&E and [B] Masson's trichrome staining). (C) Fibrosis score was evaluated as the quantity of the section positively stained for collagen and displaying alveolar wall thickening. (D) Hydroxyproline levels in lung were determined 14 days after BLM administration. Each bar represents the mean ± S.D. (C, $n = 4$; D, $n = 5$). $^{**}P < 0.01$; or $^{*}P < 0.05$ versus BLM(+), saline (i.v.).

this reaction mixture was added with DMPO (27 mM). After 6 minutes of addition of DMPO, EPR spectra were recorded at room temperature in a JES-TE-200 spectrometer (JEOL, Tokyo, Japan) under the following conditions: modulation frequency, 100 kHz; microwave frequency, 9.43 GHz; microwave power, 40 mW; scanning field, 335.2 ± 5 mT; sweep time, 2 minutes; field modulation width, 0.25 mT; receiver gain, 630; and time count, 0.3 seconds.

Radiolabeling of Proteins with ^{125}I. HSA-Trx and Trx were radiolabeled with ^{125}I according to the procedures reported previously (Watanabe et al., 2001; Furukawa et al., 2011) and purified using a Pharmacia Bio-Gel PD-10 column. The radiolabeled proteins were diluted with nonlabeled protein before conducting the pharmacokinetic experiments to adjust the dose (mg/kg) of protein in each group.

Pharmacokinetics of Trx and HSA-Trx in BLM Mice. On day 14 after BLM administration, the ^{125}I proteins (0.1 mg/kg) were injected into the tail vein of mice (~10^5 cpm/mouse). Approximately 500 μl of blood was collected from the vena cava at 0.05, 0.167, 0.5, 1, 2, 4, 6, and 12 hours after the injection of these radiolabeled proteins with the mice under ether anesthesia, and plasma was obtained. Degraded proteins and free ^{125}I were removed from plasma by centrifugation in 1% bovine serum albumin and 40% TCA. At each of these time points, the mice were sacrificed. The organs were rinsed with saline and weighed, and the ^{125}I radioactivity contained in each tissue was determined using a gamma-counter (ARC-5000; Hitachi Aloka Medical, Tokyo, Japan).

Data Analysis. Noncompartment model was used in the pharmacokinetic analyses after ^{125}I proteins administration. Each parameter was calculated using the program MOMENT (BS) (Tabata et al., 1996). Data are means ± S.D. for the indicated number of animals. Significant differences among each group were examined using a one-way of analysis of variance followed by Tukey's multiple comparison. A probability value of $P < 0.05$ was considered to indicate statistical significance.

Results

Evaluation of the Administration Schedule of HSA-Trx in BLM-Induced Pulmonary Fibrosis. Pulmonary fibrosis was induced in mice by a single intratracheal administration of BLM (day 0). Because Hoshino et al. (2003) found that the multiple administration of Trx (3.5 nmol/body) prevented BLM-induced pulmonary fibrosis, we adopted a dose of HSA-Trx equivalent to one Trx treatment (3.5 nmol/body). Figure 1 shows a schematic summary of the experimental protocols used in the study. The effect of HSA-Trx on BLM-induced pulmonary fibrosis was evaluated using H&E staining (Fig. 2A), Masson's trichrome staining (Fig. 2B), the quantity analysis of the section positively stained for collagen (Fig. 2C), and the measurement of hydroxyproline levels in lung tissue (Fig. 2D) on day 14.

H&E staining showed that BLM administration induced severe lung damage (thickened and edematous alveolar walls

and interstitia) and the infiltration of inflammatory cells into these regions (Fig. 2A). Masson's trichrome staining of collagen and the measurement of hydroxyproline levels in lung tissue indicated that BLM induced the deposition of collagen in lung (Fig. 2, B–D). These phenomena induced by BLM were all significantly suppressed by the HSA-Trx treatment. In addition, the administration of HSA-Trx at weekly intervals had a more potent effect than its use at 2-week intervals (Fig. 2, A–D). Therefore, HSA-Trx was administered once per week in the subsequent experiments.

Effect of HSA-Trx on Histologic Alterations and Hydroxyproline Levels in Lung Tissue. Hoshino et al. (2003) demonstrated that, when Trx is administered every 2 days, it prevents BLM-induced pulmonary fibrosis. Thus, we compared the effect of the intravenous administration of HSA-Trx at weekly intervals with that for the intravenous administration of Trx at weekly intervals or the intraperitoneal administration of Trx at 2-day intervals (Fig. 1B).

H&E staining (Fig. 3A), Masson's trichrome staining (Fig. 3B), the quantity analysis of the section positively stained for collagen (Fig. 3C), and hydroxyproline levels in lung tissue (Fig. 3D) clearly indicated that HSA-Trx, when administered at 1-week intervals, significantly suppressed the lung injury and fibrosis in diseased model mice. Intraperitoneal administration of Trx at 2-day intervals resulted in similar therapeutic effects as those for the HSA-Trx treatment at weekly intervals, but intravenous administration of Trx at weekly intervals showed no suppressive effect.

Effect of HSA-Trx on Active TGF-β1 Levels in Lung Tissue. TGF-β1 plays an important role in BLM-induced pulmonary fibrosis (Kinnula et al., 2005; Chaudhary et al., 2006). To reveal the mechanism underlying the suppressive effect of HSA-Trx on BLM-induced pulmonary fibrosis, the levels of active TGF-β1 in lung tissue on day 7 were determined. As shown in Fig. 4, the level of active TGF-β1 was increased in BLM mice [BLM(+), saline (i.v.)]. In contrast, HSA-Trx decreased the level of active TGF-β1 to the same level as the normal group [BLM(−)].

Effect of HSA-Trx on BALF Cells. To evaluate the effects of HSA-Trx on the inflammatory response induced by BLM, the cells in BALF were analyzed. As shown in Fig. 5, the administration of BLM resulted in an increase in the number of inflammatory cells (Fig. 5A), including alveolar macrophages (Fig. 5B), neutrophils (Fig. 5C), and lymphocytes (Fig. 5D) on days 1 and 3 after BLM administration. The HSA-Trx treatment significantly reduced the number of total cells and neutrophils on both days 1 and 3 and alveolar macrophages and lymphocytes on day 3. These results suggest that HSA-Trx ameliorates the BLM-induced pulmonary inflammatory response.

Effect of HSA-Trx on Inflammatory Cytokines and Chemokine Levels in Lung Tissue. We also examined the effect of HSA-Trx on IL-6, TNF-α, and MIF levels in the lung tissue of BLM-induced pulmonary fibrosis on days 3 and 7. As shown in Fig. 6, the levels of IL-6 (Fig. 6A), TNF-α (Fig. 6B), and MIF (Fig. 6, C and D) in lung tissue that were increased by BLM were significantly decreased as the result of the HSA-Trx treatment. These data suggest that HSA-Trx exerts an anti-inflammatory action against BLM-induced pulmonary damage.

Effect of HSA-Trx on Oxidative Stress in Lung Tissue. Recently reported findings suggest that ROS released from activated leukocytes, especially alveolar macrophages and neutrophils,

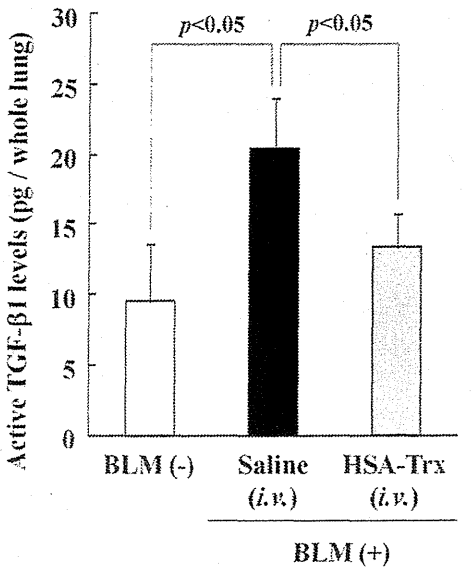

Fig. 4. Effect of HSA-Trx on active TGF-β1 levels in BLM mouse lung. Active TGF-β1 levels in lung were determined 7 days after BLM administration. Each bar represents the mean ± S.D. (n = 5).

are associated with the development of BLM-induced lung injury (Manoury et al., 2005). To evaluate the effect of HSA-Trx on the oxidative stress induced by BLM in the lung, immunostaining of 8-OH-dG and NO_2-Tyr, oxidized product of nucleic acids and proteins, respectively, and also quantification of lipoperoxidation final reaction substances, MDA, in lung sections were performed on day 3 after BLM administration. As shown in Fig. 7, the accumulation of 8-OH-dG, NO_2-Tyr, and MDA in lung tissue increased in BLM-mice [BLM(+), saline (i.v.)], compared with normal mice [BLM(−)], whereas HSA-Trx clearly suppressed the levels of these oxidative stress markers in the lungs.

To confirm whether HSA-Trx shows scavenging activity against $O_2^{\cdot-}$ generated from neutrophils, we conducted ex vivo EPR spectroscopy with use of a DMPO spin-trapping technique. As shown in Fig. 8, although PMA-stimulated neutrophils generated $O_2^{\cdot-}$ and increased EPR signaling, HSA-Trx significantly decreased the EPR signaling in a concentration-dependent manner (Fig. 8, A and B). We also compared the $O_2^{\cdot-}$ scavenging activity among HSA-Trx, Trx, and HSA. At a 30 μM concentration of each protein, HSA-Trx and Trx significantly decreased the EPR signal by 40 and 85%, respectively, whereas HSA alone did not significantly change the intensity of the signal (Fig. 8, C and D).

Effect of Post-Treatment of HSA-Trx on BLM-Induced Pulmonary Fibrosis. For future clinical applications, the postadministration effect of HSA-Trx against BLM-induced fibrosis was examined (Fig. 1C). Because HSA-Trx suppressed ROS production by neutrophils (Fig. 8), the effect of the postadministration of HSA-Trx was examined at 1 and 7 days after BLM treatment, when a marked increase in neutrophils in BALF was observed (Fig. 5C). The results of H&E staining (Fig. 9A), Masson's trichrome staining (Fig. 9B), the quantity analysis of the section positively stained for collagen (Fig. 9C), and the determination of hydroxyproline levels (Fig. 9D) on day 14 showed that the post-treatment of HSA-Trx suppressed the progression of BLM-induced fibrosis.

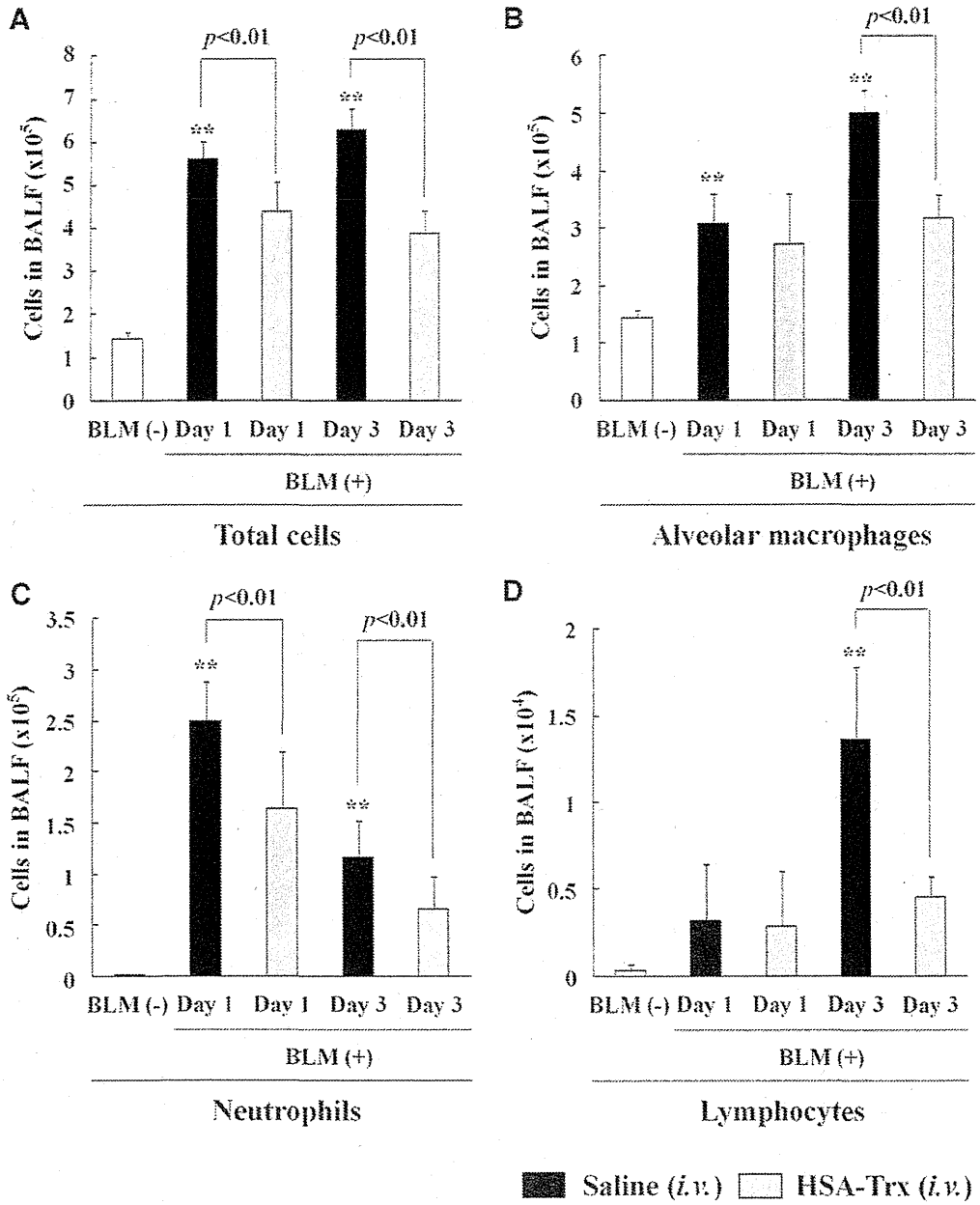

Fig. 5. Effect of HSA-Trx on BALF cells in BLM mice. Inflammatory cells number, including total cells (A), alveolar macrophages (B), neutrophils (C), and lymphocytes (D), was determined 1 and 3 days after BLM administration. Each bar represents the mean ± S.D. ($n = 6$). $^{**}P < 0.01$ versus BLM(−).

Pharmacokinetics of HSA-Trx in BLM Mice. A pharmacokinetics study of ^{125}I-labeled HSA-Trx or Trx was performed using BLM mice. As shown in Fig. 10, no significant difference between the plasma concentration-time profiles for HSA-Trx in BLM(+) mice and that in BLM(−) mice were found. The half-life of HSA-Trx was approximately 8 hours in both BLM (8.45 ± 0.85 hours) and normal (7.89 ± 0.23 hours) mice, which is more than 10 times longer than that of Trx (0.50 ± 0.02 hours) in the model mice (Fig. 10A). In addition, no significant difference was observed in the tissue distribution patterns of the HSA-Trx in BLM and normal mice, in which the highest concentration was found in the plasma, followed by the kidney, lung, spleen, and liver (Fig. 10B). On the other hand, the tissue distribution of Trx in the kidneys was the highest in BLM mice (Fig. 10B). These pharmacokinetic properties of HSA-Trx or Trx alone were similar to previously reported results using normal and ovalbumin-induced lung injury mice (Ikuta et al., 2010; Furukawa et al., 2011).

Discussion

IPF is a refractory lung disorder for which no effective treatment is available. Trx was recently shown to be present at higher concentrations in the serum and lungs of patients with IPF, compared with healthy subjects (Iwata et al., 2010). In addition, in vivo and in vitro investigations have shown that BLM treatment caused Trx to be expressed at high levels

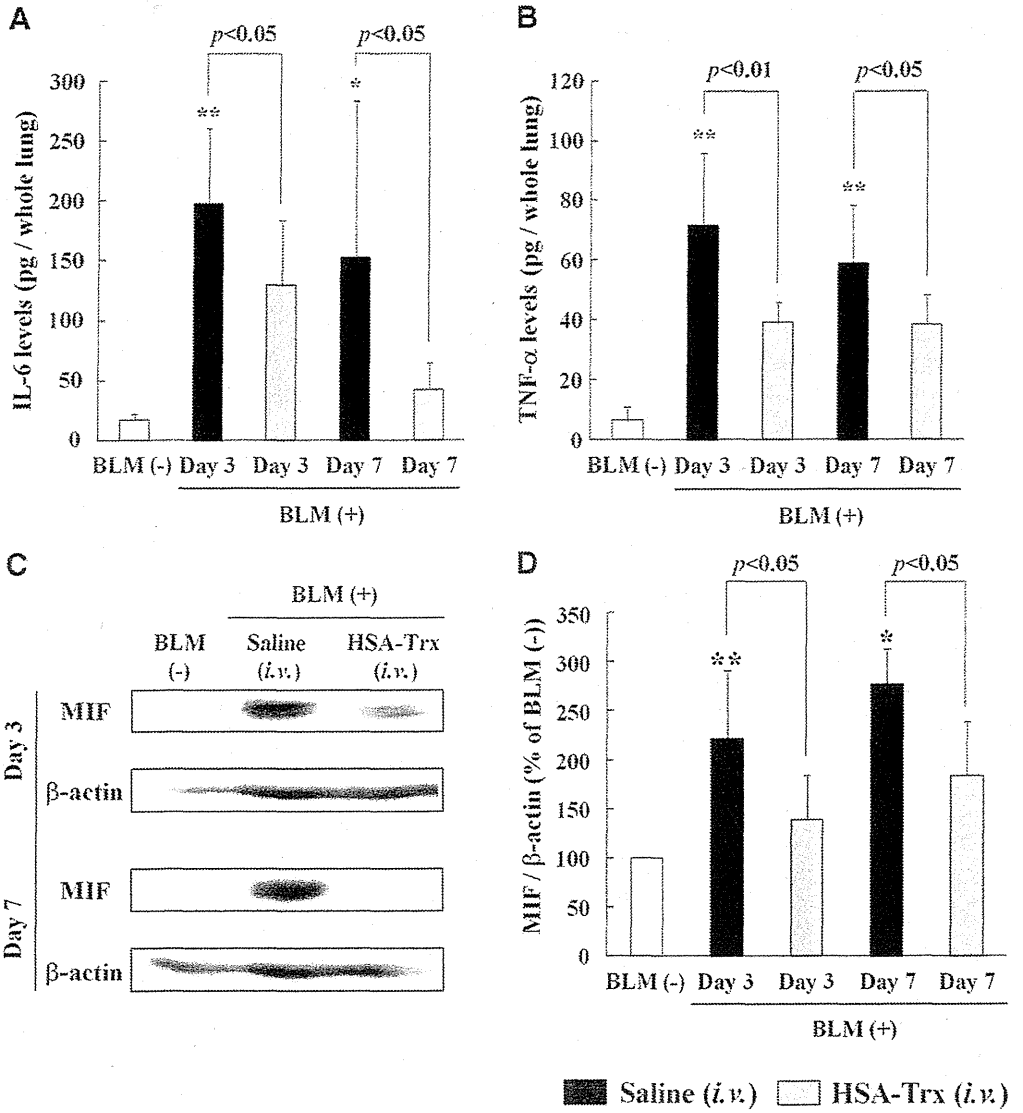

Fig. 6. Effect of HSA-Trx on pulmonary inflammatory cytokines and chemokine in BLM mice. IL-6 levels (A) and TNF-α levels (C) in lung were determined, and (C and D) MIF expression in lung were confirmed and analyzed 3 and 7 days after BLM administration. Each bar represents the mean ± S.D. (A and B, n = 5–6; D, n = 3–4). $^{**}P < 0.01$; or $^{*}P < 0.05$ versus BLM(−).

in bronchial epithelial cells, although no other endogenous antioxidative proteins (i.e., Cu/Zn-SOD, Mn-SOD, catalase, and glutathione peroxidase) were induced (Gon et al., 2001). These collective findings suggest that Trx may play an important role in the protection of lungs in patients with IPF. In this study, we evaluated the therapeutic effects of HSA-Trx on mice with BLM-induced pulmonary fibrosis and obtained four important findings. First, HSA-Trx suppressed the progression of pulmonary fibrosis when given once weekly. Second, the mechanism by which HSA-Trx inhibits lung damage induced by BLM can be attributed to the long-acting antioxidative and anti-inflammatory modulation effects of Trx. Third, the postadministration of HSA-Trx was effective in suppressing lung damage. Fourth, in the BLM-induced pulmonary fibrosis animal model, HSA-Trx exhibited similar pharmacokinetic properties to that in healthy animals (e.g., increased blood retention and enhanced distribution to the lungs).

Because the BLM-induced lung disorder animal model used in this study manifested lung disorders with a greater severity than did other conventional pathologic models, it is possible that the pathologic conditions contributed to the changes in the pharmacokinetics of HSA-Trx. However, the administration of BLM and the subsequent pulmonary fibrosis did not change the pharmacokinetic behavior of HSA-Trx (Fig. 10). This observation led to assumption that HSA-Trx could be used as a long-acting Trx that will persistently exhibit a lung-protective action in the BLM-induced lung disorders animal model. In fact, consistent with the results reported by Hoshino et al. (2003), we found that the intravenous administration of Trx at weekly intervals did not prevent pulmonary fibrosis because of its short half-life, whereas the once weekly intravenous administration of HSA-Trx suppressed the progression of fibrosis to the same extent as the intraperitoneal administration of Trx at 2-day intervals (Fig. 3). Such a reduction in the dose-frequency of Trx by fusing the protein

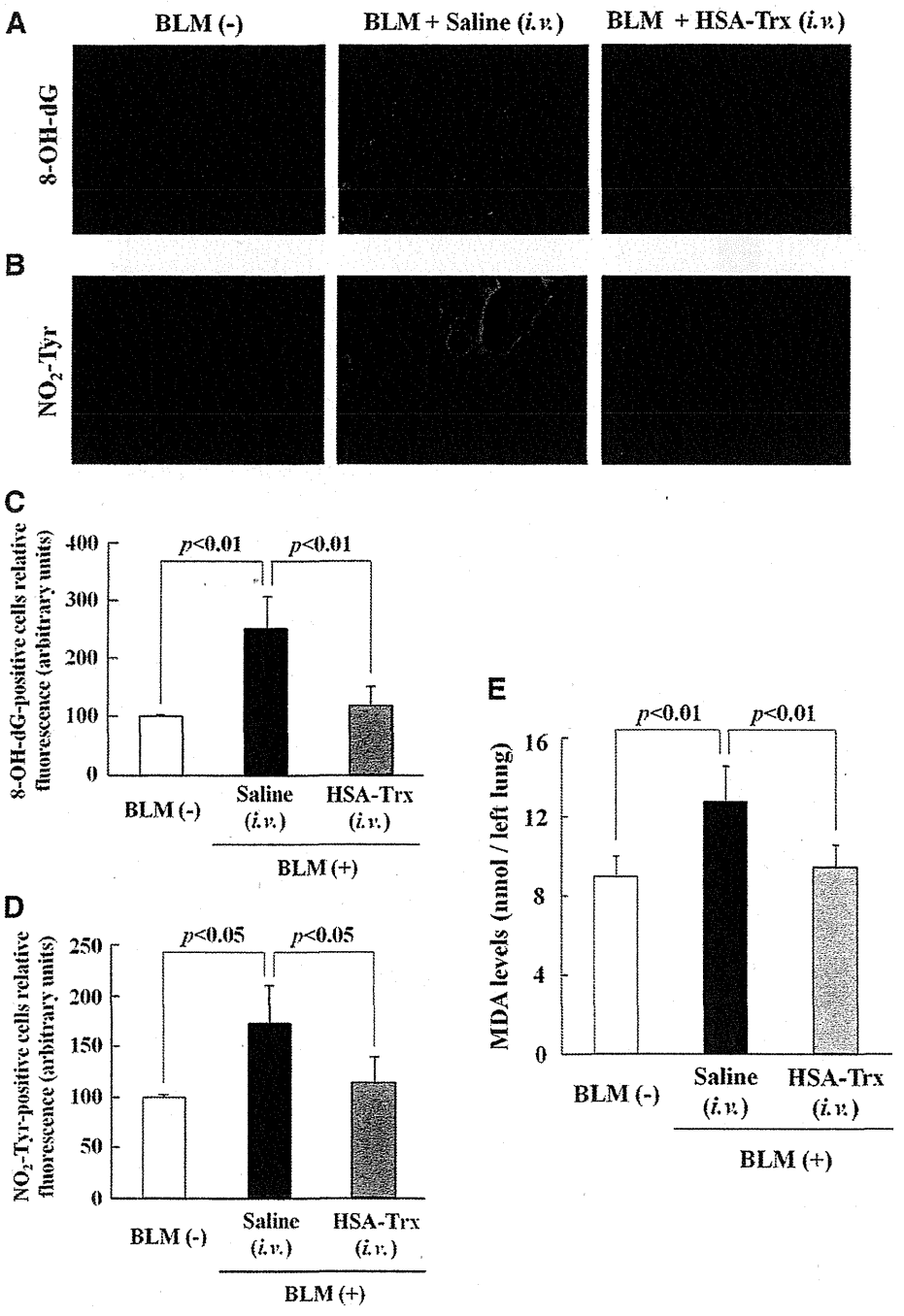

Fig. 7. Effect of HSA-Trx on pulmonary oxidative stress in BLM mice. The immunostaining of the frozen lungs slice for the oxidative stress markers of nucleic acid 8-OH-dG and amino acid (A) NO_2-Tyr (B) were performed 3 days after BLM administration. Image analysis of the extent and intensity of 8-OH-dG (C) and NO_2-Tyr (D) staining was performed. (E) The MDA levels in lung were determined 3 days after BLM administration. Each bar represents the mean ± S.D. (C and D, n = 4; E, n = 6).

to HSA is a favorable outcome from the view point of clinical applications. To the best of our knowledge, this is the first demonstration of HSA-Trx being used as an effective long-acting therapeutic agent against BLM-induced lung disordered models.

BLM-induced pulmonary fibrosis is a pathologic condition in which ROS is produced at an early stage of BLM treatment, serves as a key trigger to cause the further production of ROS that, in turn, promotes inflammatory cell infiltration and the associated secretion of inflammatory cytokines, resulting in the progression of lung injury and inflammation and, eventually, fibrosis. The suppressive effect of HSA-Trx on BLM-induced pulmonary fibrosis could be attributable to the antioxidative activity of Trx, because Trx exhibits superior antioxidative characteristics via a redox reaction of SH and S-S at its active site (Holmgren, 1989). In fact, we found that HSA-Trx significantly suppressed the accumulation of oxidative stress markers in the lungs (8-OH-dG, NO_2-Tyr and MDA) at day 3 of a BLM treatment (Fig. 7). Another investigation involving EPR experiments using a DMPO spin trapping agent examined the direct scavenging capacity of HSA-Trx for neutrophil-derived ROS, revealing the concentration-dependent suppression of $O_2^{\cdot-}$ production by HSA-Trx (Fig. 8).

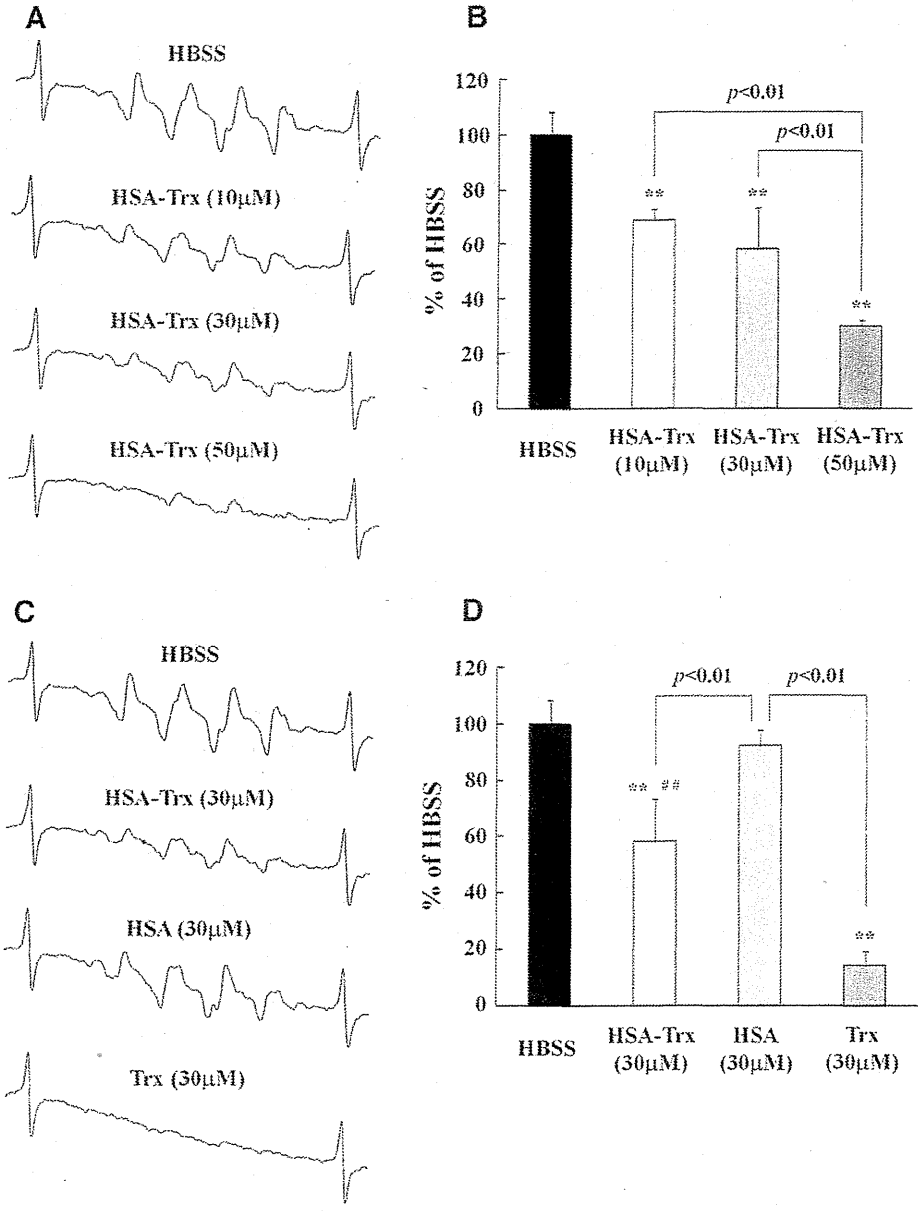

Fig. 8. Effect of HSA-Trx on neutrophil-derived ROS using EPR spectroscopy. The concentration-dependent scavenging activity of HSA-Trx against ROS released from neutrophils was determined using EPR spin trapping with DMPO. EPR spectrum of DMPO spin adducts of ·HO (A), and the quantitation of the ·HO concentration (B) were shown. The scavenging activity of HSA-Trx, HSA, and Trx (30 μM) against ROS released from neutrophils was determined by EPR spin trapping with DMPO. EPR spectrum of DMPO spin adducts of ·HO (C), and the quantitation of the ·HO concentration (D) were shown. Each bar represents the mean ± S.D. ($n = 3$). $^{**}P < 0.01$ versus Hanks' balanced salt solution (HBSS); or $^{\#\#}P < 0.01$ versus Trx.

Inflammatory cells, such as activated leukocytes, especially neutrophils, are considered to be major contributors to the onset and progression of IPF and BLM-induced pulmonary fibrosis because of their dramatic increases at the beginning of inflammation (Fig. 5C) and subsequent release of a large amount of $O_2^{\cdot-}$ (Manoury et al., 2005; Kinder et al., 2008). A comparison of the neutrophil-produced $O_2^{\cdot-}$ scavenging capacities of HSA-Trx and Trx showed that HSA-Trx retained ~ 50% of the specific activity of Trx (Fig. 8). This reduced activity of HSA-Trx is likely to be attributable to microenvironmental changes in the active center of Trx or steric hindrance as the result of the formation of a fusion complex (Muller et al., 2007).

TGF-β1 promotes interstitial collagen production via fibroblast activation and epithelial cell transition to mesenchymal cells (epithelial-mesenchymal transition) (Willis and Borok, 2007). A recent in vitro study showed that ROS and inflammatory cytokines promoted TGF-β1 production by pulmonary epithelial cells and its activation (Barcellos-Hoff and Dix, 1996; Bellocq et al., 1999). Because HSA-Trx scavenges ROS, it should be able to suppress the production of active TGF-β1 in lung tissue. The findings reported here indicate that HSA-Trx significantly reduced the active TGF-β1 content in lung tissue induced by the BLM treatment (Fig. 4). Therefore, the results suggest that the suppression of ROS production and inflammatory cell infiltration at an early-stage of BLM treatment by HSA-Trx eventually led to the suppression of active TGF-β1 production.

Active TGF-β1, in turn, activates NADPH oxidase in fibroblasts, thereby enhancing ROS production and downregulating the expression of glutamate cysteine ligase (Thannickal and Fanburg, 1995; Arsalane et al., 1997), resulting in aggravation of the redox balance in the body. It is therefore necessary to block the vicious circle of oxidative stress caused by active TGF-β1 to suppress BLM-induced pulmonary fibrosis.

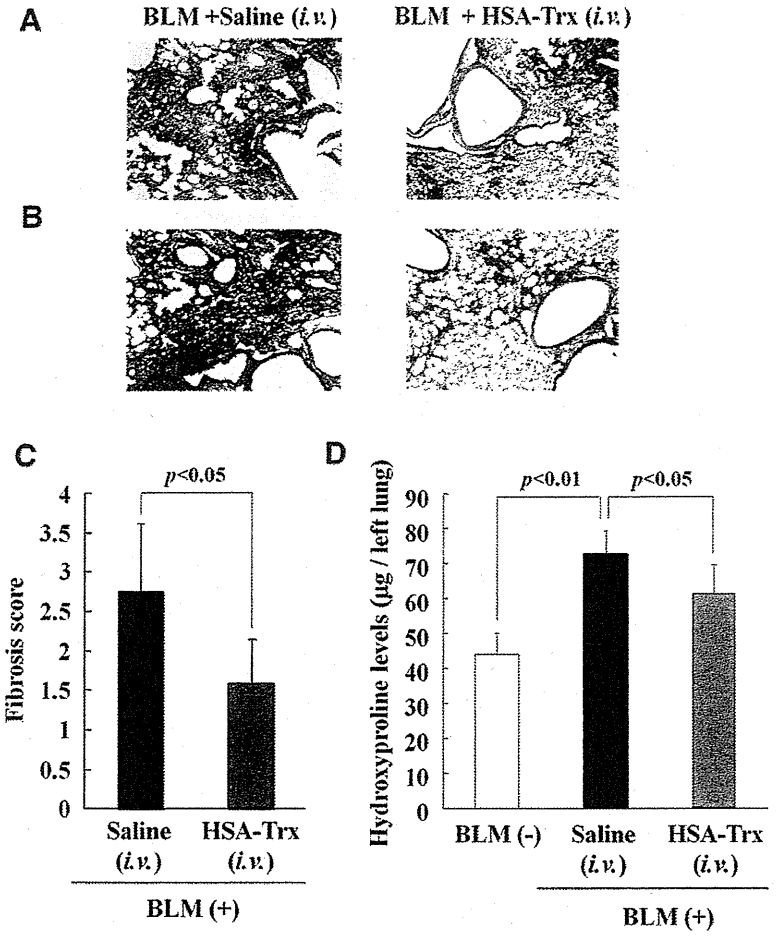

Fig. 9. Effects of postadministration of HSA-Trx (every 1 week) against BLM-induced pulmonary fibrosis 1 day after BLM treatment. (A and B) Sections of pulmonary tissue were prepared 14 days after BLM administration and subjected to histopathological examination ([A] H&E and [B] Masson's trichrome staining). (C) Fibrosis score was evaluated as the quantity of the section positively stained for collagen and displaying alveolar wall thickening. (D) Hydroxyproline levels in lung were determined 14 days after BLM administration. Each bar represents the mean ± S.D. (C, $n = 4$; D, $n = 5$).

Because weekly administration of HSA-Trx produced a better suppressing effect on pulmonary fibrosis than the fortnightly administration of HSA-Trx (Fig. 2), the ROS-scavenging action of HSA-Trx administered after the 7 days of BLM treatment may inhibit this vicious circle.

In addition to its antioxidative action, Trx has anti-inflammatory characteristics, including its ability to suppress the migration and/or infiltration and extravascular leakage of inflammatory cells (Nakamura et al., 2001). Therefore, it is highly possible that the anti-inflammatory actions of Trx are involved in the therapeutic effects of HSA-Trx against BLM-induced lung injury. In fact, HSA-Trx suppressed the pulmonary infiltration of inflammatory cells at days 1 and 3 of the administration of BLM (Fig. 5). The anti-inflammatory effects of Trx can be attributed mainly to suppression of the production of cytokines and chemokines. We also found that HSA-Trx significantly decreased the lung concentrations of these cytokines in mice with BLM-induced lung disorders (Fig. 6, A and B). Although the mechanism of suppression by Trx on the production of these cytokines remains somewhat unclear, an interesting observation was recently reported that Trx exhibited its anti-inflammatory effect by suppressing the expression and activity of MIF (Tamaki et al., 2006; Son et al., 2009). MIF promotes the production of TNF-α, IL-6, and other cytokines, as well as ROS, such as nitric oxide and superoxide anions (Baugh and Bucala, 2002). MIF is expressed at increased levels in a broad range of oxidative stress situations and inflammation-related pathologic conditions, such as sepsis, rheumatoid arthritis, inflammatory bowel disease, and lung disorders, including BLM-induced pulmonary fibrosis (Tanino et al., 2002). Furthermore, the administration of a MIF-neutralizing antibody has been shown to improve survival rates by significantly suppressing the pulmonary infiltration of inflammatory cells and the development of lung disorders (Tanino et al., 2002). It is noteworthy that HSA-Trx was also able to significantly suppress MIF expression induced by BLM administration (Fig. 6, C and D). Taking all these findings into consideration, the inactivation of MIF by HSA-Trx may also involve the anti-inflammatory effects of HSA-Trx observed in this study.

The findings of this study indicate that the progression of lung injury in a BLM-induced lung disorder mice model could be suppressed by the pre- or postadministration of HSA-Trx, demonstrating its potential as a novel therapeutic agent for the treatment of IPF, acute interstitial pneumonia, or drug-induced lung diseases. HSA-Trx may function as a long acting antioxidative and anti-inflammatory modulator. In recent years, acute exacerbation of IPF due to conditions, such as a cold or influenza, along with its progression, have contributed to the mortality among patients with IPF, and preventing acute exacerbation has been a key strategy for the treatment of the disease. Because HSA-Trx suppressed lung disorders, even when administered after BLM treatment, it is speculated that HSA-Trx may be effective in the prevention and treatment of the acute exacerbation associated with IPF.

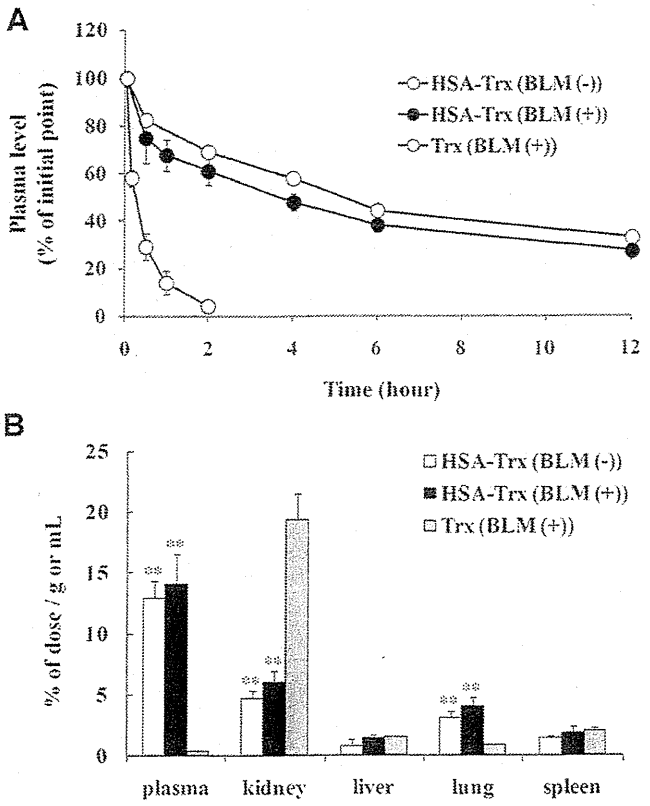

Fig. 10. Pharmacokinetic profiles of HSA-Trx and Trx and in BLM mice. (A) Plasma levels of ^{125}I-labeled HSA-Trx and Trx after intravenous administration into the tail vein of BLM and normal mice. Each point represents mean ± S.D. (n = 3). (B) Tissue distribution profile of HSA-Trx and Trx in kidney, liver, lung, and spleen at 2 hours after intravenous administration into the tail vein of BLM and normal mice. Each bar represents the mean ± S.D. (n = 3). $^{**}P < 0.01$ versus Trx [BLM(+)].

Although HSA-Trx exhibited similar blood retention levels as HSA in the BLM-induced lung disorders animal model, it is speculated to have a therapeutic effect in patients with IPF with a possibility of fortnightly or monthly administrations, considering the fact that the half-life of HSA in humans is approximately 20 days (Peters, 1985). Although further investigations related to establishing the treatment regimen need to be performed, a reduced administration frequency and stable therapeutic effect of HSA-Trx would make the treatment more convenient, safe, and cost-effective and improve the health-related quality of life for patients with IPF. The BLM animal model is widely used in the assessment of potential antifibrotic agents. However, the aspect of slow and irreversible progression of IPF in patients is not reproduced in the BLM model. It would be interesting to see whether this therapeutic could reverse or slow progression of fibrosis in the clinical setting as opposed to preventing the response evoked by BLM.

Authorship Contributions

Participated in research design: R. Tanaka, Watanabe, Kodama, Chuang, Ishima, Hamasaki, K. Tanaka, Mizushima, Otagiri, Maruyama.

Conducted experiments: R. Tanaka, Watanabe, Kodama, Ishima.

Contributed new reagents or analytic tools: R. Tanaka, Watanabe, Kodama.

Performed data analysis: R. Tanaka, Watanabe, Kodama.

Wrote or contributed to writing of the manuscript: R. Tanaka, Watanabe, Chuang, Otagiri, Maruyama.

References

American Thoracic Society and the European Respiratory Society (2000) American Thoracic Society. Idiopathic pulmonary fibrosis: diagnosis and treatment. International consensus statement. American Thoracic Society (ATS), and the European Respiratory Society (ERS). *Am J Respir Crit Care Med* **161**:646–664.

Arsalane K, Dubois CM, Muanza T, Bégin R, Boudreau F, Asselin C, and Cantin AM (1997) Transforming growth factor-beta1 is a potent inhibitor of glutathione synthesis in the lung epithelial cell line A549: transcriptional effect on the GSH rate-limiting enzyme gamma-glutamylcysteine synthetase. *Am J Respir Cell Mol Biol* **17**:599–607.

Barcellos-Hoff MH and Dix TA (1996) Redox-mediated activation of latent transforming growth factor-beta 1. *Mol Endocrinol* **10**:1077–1083.

Baugh JA and Bucala R (2002) Macrophage migration inhibitory factor. *Crit Care Med* **30**:27–35.

Beeh KM, Beier J, Haas IC, Kornmann O, Micke P, and Buhl R (2002) Glutathione deficiency of the lower respiratory tract in patients with idiopathic pulmonary fibrosis. *Eur Respir J* **19**:1119–1123.

Bellocq A, Azoulay E, Marullo S, Flahault A, Fouqueray B, Philippe C, Cadranel J, and Baud L (1999) Reactive oxygen and nitrogen intermediates increase transforming growth factor-beta1 release from human epithelial alveolar cells through two different mechanisms. *Am J Respir Cell Mol Biol* **21**:128–136.

Chaudhary NI, Schnapp A, and Park JE (2006) Pharmacologic differentiation of inflammation and fibrosis in the rat bleomycin model. *Am J Respir Crit Care Med* **173**:769–776.

Chen RF (1967) Removal of fatty acids from serum albumin by charcoal treatment. *J Biol Chem* **242**:173–181.

Fattman CL, Chang LY, Termin TA, Petersen L, Enghild JJ, and Oury TD (2003) Enhanced bleomycin-induced pulmonary damage in mice lacking extracellular superoxide dismutase. *Free Radic Biol Med* **35**:763–771.

Flaherty KR, Travis WD, Colby TV, Toews GB, Kazerooni EA, Gross BH, Jain A, Strawderman RL, Flint A, and Lynch JP, et al. (2001) Histopathologic variability in usual and nonspecific interstitial pneumonias. *Am J Respir Crit Care Med* **164**: 1722–1727.

Furukawa M, Tanaka R, Chuang VT, Ishima Y, Taguchi K, Watanabe H, Maruyama T, and Otagiri M (2011) Human serum albumin-thioredoxin fusion protein with long blood retention property is effective in suppressing lung injury. *J Control Release* **154**:189–195.

Gibbons MA, MacKinnon AC, Ramachandran P, Dhaliwal K, Duffin R, Phythian-Adams AT, van Rooijen N, Haslett C, Howie SE, and Simpson AJ, et al. (2011) Ly6Chi monocytes direct alternatively activated profibrotic macrophage regulation of lung fibrosis. *Am J Respir Crit Care Med* **184**:569–581.

Gon Y, Sasada T, Matsui M, Hashimoto S, Takagi Y, Iwata S, Wada H, Horie T, and Yodoi J (2001) Expression of thioredoxin in bleomycin-injured airway epithelium: possible role of protection against bleomycin induced epithelial injury. *Life Sci* **68**:1877–1888.

Holmgren A (1989) Thioredoxin and glutaredoxin systems. *J Biol Chem* **264**:13963–13966.

Hoshino T, Nakamura H, Okamoto M, Kato S, Araya S, Nomiyama K, Oizumi K, Young HA, Aizawa H, and Yodoi J (2003) Redox-active protein thioredoxin prevents proinflammatory cytokine- or bleomycin-induced lung injury. *Am J Respir Crit Care Med* **168**:1075–1083.

Ikuta S, Chuang VT, Ishima Y, Nakajou K, Furukawa M, Watanabe H, Maruyama T, and Otagiri M (2010) Albumin fusion of thioredoxin—the production and evaluation of its biological activity for potential therapeutic applications. *J Control Release* **147**:17–23.

Iwata Y, Okamoto M, Hoshino T, Kitasato Y, Sakazaki Y, Tajiri M, Matsunaga K, Azuma K, Kawayama T, and Kinoshita T, et al. (2010) Elevated levels of thioredoxin 1 in the lungs and sera of idiopathic pulmonary fibrosis, non-specific interstitial pneumonia and cryptogenic organizing pneumonia. *Intern Med* **49**:2393–2400.

Keane MP and Strieter RM (2002) The importance of balanced pro-inflammatory and anti-inflammatory mechanisms in diffuse lung disease. *Respir Res* **3**:5.

Kinder BW, Brown KK, Schwarz MI, Ix JH, Kervitsky A, and King TE, Jr (2008) Baseline BAL neutrophilia predicts early mortality in idiopathic pulmonary fibrosis. *Chest* **133**:226–232.

Kinnula VL, Fattman CL, Tan RJ, and Oury TD (2005) Oxidative stress in pulmonary fibrosis: a possible role for redox modulatory therapy. *Am J Respir Crit Care Med* **172**:417–422.

Liu W, Nakamura H, Shioji K, Tanito M, Oka S, Ahsan MK, Son A, Ishii Y, Kishimoto C, and Yodoi J (2004) Thioredoxin-1 ameliorates myosin-induced autoimmune myocarditis by suppressing chemokine expressions and leukocyte chemotaxis in mice. *Circulation* **110**:1276–1283.

Luppi F, Cerri S, Beghè B, Fabbri LM, and Richeldi L (2004) Corticosteroid and immunomodulatory agents in idiopathic pulmonary fibrosis. *Respir Med* **98**: 1035–1044.

Manoury B, Nenan S, Leclerc O, Guenon I, Boichot E, Planquois JM, Bertrand CP, and Lagente V (2005) The absence of reactive oxygen species production protects mice against bleomycin-induced pulmonary fibrosis. *Respir Res* **6**:11.

Moore BB and Hogaboam CM (2008) Murine models of pulmonary fibrosis. *Am J Physiol Lung Cell Mol Physiol* **294**:L152–L160.

Müller D, Karle A, Meissburger B, Höfig I, Stork R, and Kontermann RE (2007) Improved pharmacokinetics of recombinant bispecific antibody molecules by fusion to human serum albumin. *J Biol Chem* **282**:12650–12660.

Nakamura H, Herzenberg LA, Bai J, Araya S, Kondo N, Nishinaka Y, Herzenberg LA, and Yodoi J (2001) Circulating thioredoxin suppresses lipopolysaccharide-induced neutrophil chemotaxis. *Proc Natl Acad Sci USA* **98**:15143–15148.

Nakamura T, Nakamura H, Hoshino T, Ueda S, Wada H, and Yodoi J (2005) Redox regulation of lung inflammation by thioredoxin. *Antioxid Redox Signal* **7**:60–71.

Peters T, Jr (1985) Serum albumin. *Adv Protein Chem* **37**:161–245.

Piguet PF, Collart MA, Grau GE, Kapanci Y, and Vassalli P (1989) Tumor necrosis factor/cachectin plays a key role in bleomycin-induced pneumopathy and fibrosis. *J Exp Med* **170**:655–663.

JPP JOURNAL OF Pharmacy and Pharmacology
ROYAL PHARMACEUTICAL SOCIETY
JPP Journal of Pharmacy And Pharmacology
Research Paper

Prostaglandin E_1-containing nanoparticles improve walking activity in an experimental rat model of intermittent claudication

Tomoaki Ishihara[a], Yasunobu Yamashita[a], Naoko Takasaki[b], Shuhei Yamamoto[b], Erika Hayashi[a], Kayoko Tahara[c], Mitsuko Takenaga[d], Naoki Yamakawa[a,b], Tsutomu Ishihara[e], Tadashi Kasahara[a] and Tohru Mizushima[a]

[a]Faculty of Pharmacy, Keio University, Tokyo, [b]Graduate School of Medical and Pharmaceutical Sciences, Kumamoto University, Kumamoto, [c]Faculty of Pharmacy, Health Sciences University of Hokkaido, Hokkaido, [d]Division of Drug Delivery System, Institute of Medical Science, St. Marianna University, Kawasaki and [e]Department of Chemical Biology and Applied Chemistry, College of Engineering, Nihon University, Fukushima, Japan

Keywords
biodegradable nanoparticles; encapsulation; intermittent claudication; prostaglandin E_1; quality of life

Correspondence
Tohru Mizushima, Department of Analytical Chemistry, Faculty of Pharmacy, Keio University, 1-5-30, Shibakoen, Minato-ku, Tokyo 105-8512, Japan.
E-mail: mizushima-th@pha.keio.ac.jp

Received January 31, 2013
Accepted April 16, 2013

doi: 10.1111/jphp.12080

Abstract

Objectives Due to the low stability of lipid emulsions, a lipid emulsion of prostaglandin E_1 (Lipo-PGE_1) necessitates daily intravenous drip infusions. To overcome this issue, we developed nanoparticles containing PGE_1 (Nano-PGE_1). Nano-PGE_1 showed a good sustained-release profile of PGE_1 from the nanoparticles *in vitro*, which may permit a longer-lasting therapeutic effect to be achieved. We here examined the pharmacological activity of Nano-PGE_1 in a rat experimental model of intermittent claudication induced by femoral artery ligation.

Methods The walking activity of the rat was tested on a rodent treadmill. Tissue levels of PGE_1 were determined by enzyme immunoassay, and skeletal muscle angiogenesis (capillary growth) was monitored by immunohistochemical analysis.

Key findings PGE_1 could be detected in the lesion site one day after the intravenous administration of Nano-PGE_1 but not of Lipo-PGE_1. An increased accumulation of Nano-PGE_1 in the lesion site compared with control (unlesioned) site was also observed. The ligation procedure reduced the walking activity, which in turn was improved by a single administration of Nano-PGE_1 but not of Lipo-PGE_1. The single administration of Nano-PGE_1 also stimulated angiogenesis in the skeletal muscle around the ligated artery.

Conclusions The findings of this study suggest that Nano-PGE_1 improves the walking activity of femoral artery-ligated rats through the accumulation and sustained release of PGE_1.

Introduction

Peripheral arterial disease (PAD) forms part of the more extensive vascular problem of atherosclerosis. The number of patients with PAD has increased in line with ageing of the population.[1–3] PAD increases the risk of cardiovascular and cerebrovascular events, such as myocardial infarction, ischaemic stroke and vascular death.[2,4,5] Lower-limb amputation is also a common outcome in advanced PAD, drastically decreasing walking activity and the quality of life (QOL) of affected patients. While various clinical treatments, such as vascular bypass surgery, have been developed to treat severe PAD accompanied by pain at rest (critical limb ischaemia (CLI)), the prognosis is still not good and thus establishment of clinical protocol to treat CLI is very important.

Intermittent claudication (IC) with reproduced ischaemic leg pain on exercise is a common presentation in patients with mild PAD. IC is caused by skeletal muscle ischaemia due to an imbalance between the arterial blood supply and the metabolic demands of skeletal muscles in the leg.[5] Although most IC patients do not require surgical

intervention, the prognosis for the condition is not good due to the high risk of cardiovascular and cerebrovascular events. Most patients must receive medical therapy, focusing on not only reducing the incidence of cardiovascular and cerebrovascular events, but also improving the QOL of patients by reducing ischaemia through improved peripheral blood flow. The initial approach for the treatment of IC is structured exercise and, in selected patients, pharmacotherapy.

Prostaglandin (PG) E_1, which has various physiological actions, such as vasodilatation, angiogenesis and inhibition of platelet aggregation, serves as an effective treatment for PAD.[6–8] However, when administered systemically, PGE_1 has related adverse effects such as hypotension and diarrhoea.[9,10] Furthermore, in addition to its chemical instability (hydrolysis to PGA_1), PGE_1 is easily inactivated by 15-hydroxydehydrogenase during its passage through the lung.[11–13] To overcome these obstacles, Lipo-PGE_1, a preparation incorporating PGE_1 into an oil-in-water lipid emulsion, has been developed.[14–16] Incorporation of PGE_1 into the lipid emulsion protects PGE_1 from inactivation in the lung and enables the selective delivery of PGE_1 to damaged blood vessels, resulting in enhanced therapeutic effects and reduced drug-related toxicity.[14,17] Lipo-PGE_1 has been approved for clinical use in Japan, Korea and China to treat CLI; however, the effectiveness of PGE_1-related drugs in CLI is still open to argument.[2,18] Lipo-PGE_1 is unable to retain PGE_1 for a long period,[19,20] meaning that daily intravenous drip infusions are necessary. A major disadvantage of Lipo-PGE_1, therefore, is that its clinical use requires patient hospitalization and lowers their QOL. A new formulation of PGE_1 that enables the sustained release of PGE_1 would be highly beneficial.

Nanoparticles, such as liposomes and polymeric solid particles that are approximately 100–200 nm in diameter, have been widely used as carrier systems for targeted drug delivery to tumours, inflammatory tissues and vascular lesions due to their enhanced permeability and retention (EPR) effects.[21] However, particles of this size are easily captured by the mononuclear phagocyte system (MPS), resulting in their rapid clearance from the circulation.[22,23] Modification of the nanoparticle surface with polyethyleneglycol (PEG) enables such nanoparticles to escape this uptake via a 'stealth effect'.[20,22,23]

We recently developed a novel formulation of PGE_1 in which the PGE_1 is encapsulated in biodegradable and biocompatible polymeric solid particles prepared with a polylactide (PLA) homopolymer and a monomethoxy PEG–PLA block copolymer (PEG-PLA). These particles have a mean diameter of 120 nm, which enhances the selective delivery of PGE_1 to damaged blood vessels due to the EPR effect.[20] We also achieved a good sustained-release profile of PGE_1 from the nanoparticles along with degradation of the polymers *in vitro*, which may permit a longer-lasting therapeutic effect to be achieved.[20] Based on these data, we proposed that PGE_1-containing PEG-modified PLA nanoparticles (Nano-PGE_1) would be of significant clinical benefit if a single administration of this formulation could maintain a desired level of PGE_1 around damaged blood vessels for 1–2 weeks. In other words, administration of this formulation to IC patients at 1- to 2-week intervals may help improve symptoms without requiring patients to undergo frequent hospitalization.

Here, we examine the pharmacological activity of Nano-PGE_1 in an experimental rat model of IC induced by femoral artery ligation. Results show not only that PGE_1 is targeted to the lesion site more efficiently with Nano-PGE_1 than with Lipo-PGE_1, but also that Nano-PGE_1 improves femoral artery ligation-reduced walking activity more efficiently than Lipo-PGE_1. This is the first time that the pharmacological activity of Nano-PGE_1 has been tested in experimental animal models related to PAD.

Materials and Methods

Materials and animals

PGE_1 was purchased from Nissan Chemical Industries, Ltd (Tokyo, Japan). Poly (L-lactide) (L-PLA) (Mw = 20, 000) was from Taki Chemical Co. Ltd (Kakogawa, Japan). Poly (D,L-lactic acid) (D,L-PLA) (Mw = 20, 000), iron chloride and 1,4-dioxane were purchased from Wako Pure Chemicals Industries Ltd (Osaka, Japan). PEG-D, L-PLA (average molecular weight of PEG and PLA are 5600 and 9400, respectively) was synthesized and evaluated as described previously.[20] Wistar rats (6 weeks old) were from Kyudo Co. Ltd (Kumamoto, Japan). The rats were allowed free access to water and rat chow, and were housed under controlled environmental conditions (constant temperature, humidity and a 12-h dark–light cycle). The experiments and procedures described here were carried out in accordance with the Guide for the Care and Use of Laboratory Animals as adopted and promulgated by the National Institutes of Health, and were approved by the Animal Care Committee of Keio University on 1 June 2011 (licence number: 11010-(0)) and Kumamoto University on 30 March 2012 (licence number: C 24–236).

Preparation of nanoparticles

Nanoparticles were prepared by using the oil-in-water solvent diffusion method as described previously.[20,24] L-PLA or D,L-PLA in 1,4-dioxane was mixed with PGE_1, PEG-D, L-PLA, iron chloride and diethanolamine (DEA) in acetone (the total amount of block copolymers and homopolymer was fixed at 25 mg). Samples were incubated for 10 min at room temperature and added to 25 ml of

© 2013 Royal Pharmaceutical Society, *Journal of Pharmacy and Pharmacology*, 65, pp. 1187–1194

Milli-Q water stirred at 1000 rpm. After addition of 0.5 ml of 0.5 M EDTA (pH 7.0) and 12.5 μl of 200 mg/ml Tween 80, nanoparticles were purified and concentrated. We named the nanoparticles based on the isomer and molecular weight of PLA, such as NP-L20 and NP-DL20. 'NP' indicates nanoparticles, 'L' or 'DL' indicates L-PLA or D, L-PLA, respectively; '20' means that PLA with molecular weight of 20 000 was used for preparation of NP. Thus, NP-L20 is NPs prepared with L-PLA of molecular weight 20 000. NP-L20 is a representative Nano-PGE_1, which was shown in a previous study to have high stability both *in vivo* and *in vitro* (its half-life in solutions containing serum is about 1 week).[20] We also reported characteristic features of NP-L20 (size distribution, 117 ± 8 nm; loading efficacy, 1.33 ± 0.12%; polydispersity index, 0.075; half-life after injection, 10.2 ± 0.2 h).[20] On the other hand, although NP-DL20 has a particle size similar to that of NP-L20, it is unstable both *in vivo* and *in vitro* (the half-life of NP-DL20 in solutions containing serum is less than 1 day).[20] We also reported characteristic features of NP-DL20 (size distribution, 121 ± 7 nm; loading efficacy, 1.22 ± 0.11%; polydispersity index, 0.088; half-life after injection, 6.0 ± 0.7 h).[20] We used both NP-L20 and NP-DL20 in experiments in this study.

A lipid emulsion incorporating PGE_1 (Lipo-PGE_1) was prepared according to the published method.[25] Nano-PGE_1 or Lipo-PGE_1 was administered via the tail vein (10 ml/kg).

Femoral artery ligation model and treadmill walking test

Experiments were performed as described previously.[26] Male Wistar rats (6 weeks old) were used in the experiments after acclimatization for at least 1 week. During the acclimatization period, rats were trained to walk on a rodent treadmill (Model MK-680; Muromachi kikai Co., Ltd, Tokyo, Japan) under the following conditions: over the first 2 days, sessions were carried out with the rats walking at a slope angle of 0° and a belt speed of 20 m/min for 3 min and then at 25 m/min for 7 min; for the following 5 days, a slope angle of 10° and a belt speed of 25 m/min for 12 min were used. The variation of treadmill test conditions (slope angle and belt speed) is because rats are trained to walk well in the first 2 days.[27] Walking distance was defined as the total distance walked until the hind paw of the rat had received five mild electrical stimulations (measurement started 1 min after the commencement of walking). The walking distance for rats that received less than five electrical stimulations was estimated as 300 m.

Rats satisfying the walking distance of 300 m were subjected to femoral artery ligation on day 0. Rats were anaesthetized with pentobarbital sodium (50 mg/kg, i.p.) and a vertical longitudinal incision was made on both hindlimbs. The femoral artery on each side was exposed and ligated with silk suture (2 cm) and completely excised by this incision. One day after the ligation (day 1), walking distance was evaluated according using the method described above. Those rats not capable of walking more than 100 m were randomly assigned to different experimental groups. Treadmill walking tests were performed again on days 4, 8 and 15.

Cuff-induced arterial neointimal formation model

The surgical procedures for cuff placement were performed as described previously.[28] Briefly, rats were anaesthetized with pentobarbital (50 mg/kg, i.p.) and the femoral artery was isolated. A polyethylene tube (PE-160, 1.5 cm long, inner diameter of 1.14 mm, outer diameter of 1.57 mm; Becton Dickinson and Company, Franklin Lakes, NJ, USA) was loosely placed the around the artery.

Distribution of each formulation of PGE_1 to the lesion site

Femoral and gastrocnemius muscles (femoral artery ligation model) or femoral muscles only (cuff-induced arterial neointimal formation model) were isolated from rats administered each type of PGE_1 formulation. Tissues were homogenized in a solution, containing 0.01 mg/ml indometacin. After freeze-thawing and the addition of 1,4-dioxane, samples were centrifuged. The supernatant fraction (200 μl) was evaporated to dryness and dissolved in 500 μl of PGE_1 enzyme immunoassay (EIA) buffer (R&D Systems Inc., Mineapolis, MN, USA). The PGE_1 content was determined using a PGE_1 EIA kit according to the manufacturer's protocol.

Morphometric analysis of capillary density

Morphometric analysis of capillary density was carried out as described,[29] with some modifications. One day after the last treadmill walking test (see above), rats were killed and perfused with saline. The white gastrocnemius muscle was embedded in optimal cutting temperature compound (Sakura Finetechnical, Tokyo, Japan) and frozen in liquid nitrogen. Cryostat sections (6 μm thick) were prepared and incubated in 0.3% hydrogen peroxide to block endogenous peroxide activity. Sections were pre-incubated for 30 min in 2.5% goat serum and then incubated with antibody against CD31 (Becton Dickinson and Company). Sections were washed and then incubated with peroxidase-labelled polymer conjugated to goat anti-mouse immunoglobulin (Dako, Carpintaria, CA, USA). After washing, sections were incubated first with the chromogen diaminobenzidine followed by hematoxylin and finally mounted with malinol. Sections were inspected using a BX51 microscope

(Olympus, Tokyo, Japan). Capillary contacts per muscle fibre were calculated by counting the total numbers of transverse capillaries and fibres in five randomly selected fields (each field measuring 90 000 μm).[12]

Statistical analysis

All values are expressed as the mean ± standard error of the mean (S.E.M.). One-way analysis of variance followed by the Tukey test or the Kruskal–Wallis test was used to evaluate differences, when the number of rats per group exceeded five or not, respectively. Differences were considered to be significant for values of $P \leq 0.05$.

Results

Accumulation of Nano-PGE_1 in the vascular lesion site

In this study, we tried to compare the pharmacological activity of Nano-PGE_1 to Lipo-PGE_1. In a first series of experiments, we examined the distribution of NP-L20, NP-DL20 and Lipo-PGE_1 around the lesion site in the rat femoral artery ligation model (Figure 1a). This experiment was different from those whose results are shown in Figures 2–4, with only the right femoral artery being ligated. As shown in Figure 1a, when Lipo-PGE_1, NP-DL20 or NP-L20 was intravenously administered 1 day after the ligation, a higher level of PGE_1 was detected in the left (control) hindlimb tissue of rats administered NP-L20 than in those administered Lipo-PGE_1 or NP-DL20. This finding may be due to the high stability of NP-L20 in serum.[20] Further to this, the level of PGE_1 was significantly higher in the right (ischaemic) hindlimb than in the left (non-ischaemic) hindlimb (Figure 1a), suggesting that NP-L20 accumulates in skeletal muscle tissues around the ligated artery.

It was reported that the placement of a cuff around an artery results in concentric intimal hyperplasia, which is also regarded as an alternative model for vascular injury associated with atherosclerosis.[28] We therefore examined the degree of accumulation of NP-L20 in the region of the cuff-injured right femoral artery, with NP-L20 intravenously administered on day 3 or 14 after the cuff placement. As shown in Figure 1b, 24 h after administration of the drug, a higher level of PGE_1 was detected in the hindlimb with cuff placement than in the control limb, suggesting that NP-L20 accumulates around the cuff-injured artery.

Effect of Nano-PGE_1 on walking disturbances induced by femoral artery ligation

The effect of NP-L20 on walking disturbance related to IC was estimated in rats by use of the femoral artery ligation

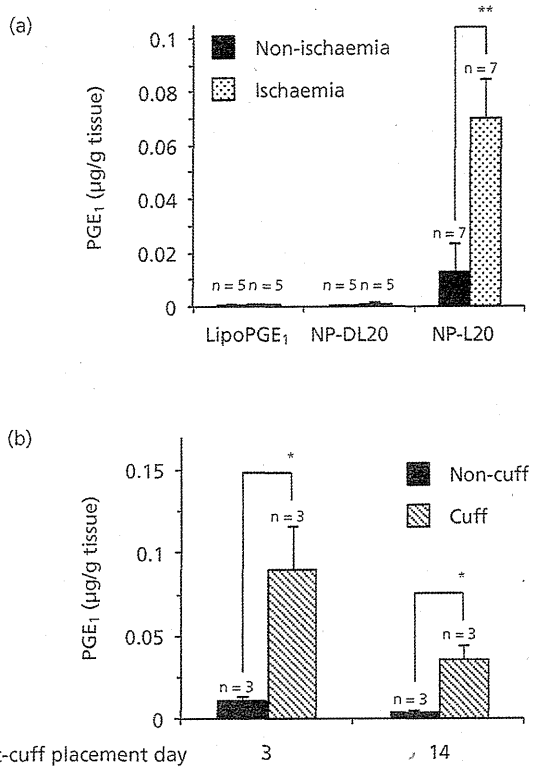

Figure 1 Accumulation of NP-L20 in the vascular lesion site of femoral artery-ligated rats. Femoral artery ligation (a) or cuff placement (b) was performed on the right femoral artery only (right, ischaemic; left, non-ischaemic). A sham operation was carried out on the left femoral artery. One day after the femoral artery ligation, or 3 or 14 days after the cuff placement, Lipo-PGE_1, NP-DL20 or NP-L20 (200 μg PGE_1/kg) was administered intravenously. Twenty-four hours after the drug administration, the levels of PGE_1 in tissue lysates were measured by EIA. Values are mean ± S.E.M. $^{**}P < 0.01$, $^{*}P < 0.05$ (a, by the Tukey test; LipoPGE1 Non-ischaemia, $n = 5$; LipoPGE1 Ischaemia, $n = 5$; NP-DL20 Non-ischaemia, $n = 5$; NP-DL20 Ischaemia, $n = 5$; NP-L20 Non-ischaemia, $n = 7$; NP-L20 Ischaemia $n = 7$; b, by the Kruskal–Wallis test; day 3 Non-cuff, $n = 3$; day 3 Cuff, $n = 3$; day 14 Non-cuff, $n = 3$; day 14 Cuff, $n = 3$).

model. One day after bilateral femoral artery ligation, rats with decreased walking behaviour (see Methods) were selected, randomly allocated into different experimental groups and intravenously administered NP-L20. The walking activity of each rat was measured by the treadmill walking test. As shown in Figure 2, the femoral artery ligation-induced walking disturbance had clearly not been recovered to normal (300 m) in vehicle-treated rats by day 15. On the other hand, NP-L20 administration resulted in a dose-dependent improvement of walking activity by day 15 (Figure 2).

We next examined the effect of Lipo-PGE_1 or NP-DL20 on the femoral artery ligation-induced walking disturbance.

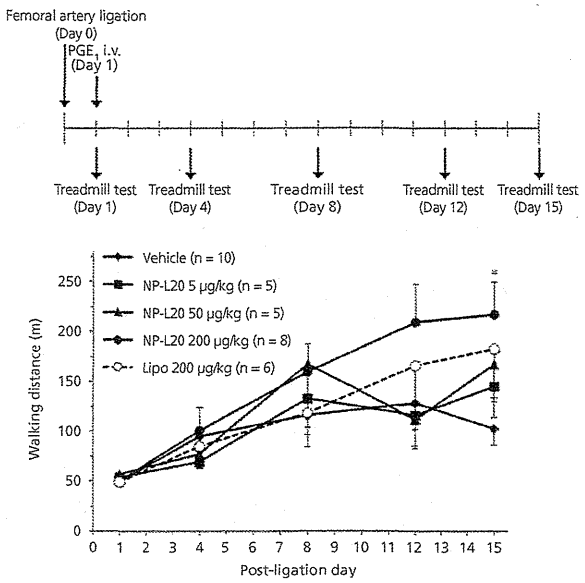

Figure 2 Effect of a single administration of NP-L20 on femoral artery ligation-induced walking disturbance in rats. Bilateral femoral artery ligation was performed on day 0 and the indicated amount (μg PGE$_1$/kg) of NP-L20 or Lipo-PGE$_1$ was administered intravenously once only on day 1. Treadmill walking tests were carried out as described in the Methods. Values are presented as the mean ± S.E.M. *$P < 0.05$ vs vehicle (by the Tukey test; Vehicle, $n = 10$; NP-L20 5 μg/kg, $n = 5$; NP-L20 50 μg/kg, $n = 5$; NP-L20,200 μg/kg, $n = 8$; Lipo 200 μg/kg, $n = 6$).

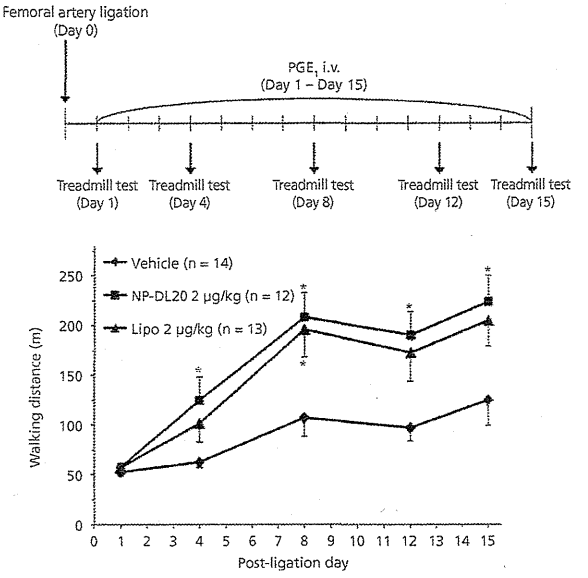

Figure 3 Effect of repeated administration of Lipo-PGE$_1$ or NP-DL20 on femoral artery ligation-induced walking disturbance in rats. Bilateral femoral artery ligation and treadmill walking tests were carried out as described in the legend of Figure 2. Indicated amounts (μg PGE$_1$/kg) of Lipo-PGE$_1$ or NP-DL20 were administered intravenously once daily from day 1 to day 14. On days when the treadmill test was carried out (day 4, 8, 12 and 15) the drug administration was performed after the treadmill walking test had been completed. Values are mean ± S.E.M. *$P < 0.05$ vs vehicle (by the Tukey test; Vehicle, $n = 14$; NP-DL20 2 μg/kg, $n = 12$; Lipo 2 μg/kg, $n = 13$).

A single administration of either Lipo-PGE$_1$ (Figure 2) or NP-DL20 (up to 50 μg/kg, data not shown) did not improve walking ability. Since Lipo-PGE$_1$ and NP-DL20 were less stable than NP-L20,[20] we assumed that these drugs may improve the walking activity with repeated administration. Thus, we examined the effect of daily administrations of these drugs. As shown in Figure 3, NP-DL20 administered daily significantly improved the walking ability. Administration of Lipo-PGE$_1$ also improved the walking ability (Figure 3).

Effect of Nano-PGE$_1$ on angiogenesis in the rat femoral artery ligation model

It has been suggested that angiogenesis induced by tissue ischaemia plays an important role in recovery from femoral artery ligation-induced walking disturbance.[30,31] We therefore examined the number of capillaries in right hindlimb (ischaemic) gastrocnemius muscles 1 day after the final treadmill walking test (see Figures 2 and 3). As shown in Figure 4a,b, a single administration of NP-L20 increased the number of capillary contacts per fibre in a dose-dependent manner. Such an increase was not observed after a single administration of Lipo-PGE$_1$ (Figure 4a,b). A similar increase was observed in rats that had been repeatedly administered NP-DL20 or Lipo-PGE$_1$ (Figure 4c,d). The results presented in Figure 4 thus suggest that NP-L20, NP-DL20 and Lipo-PGE$_1$ improve the femoral artery ligation-induced walking disturbance by stimulating the process of angiogenesis.

Discussion

In this study, using a rat model of IC induced by femoral artery ligation, we confirmed the increased accumulation of PGE$_1$, after administration of NP-L20, in tissue around the ligated femoral artery site with respect to control tissue. Under the same experimental conditions, PGE$_1$ could not be detected clearly when Lipo-PGE$_1$ was used as the means of drug delivery. Furthermore, with NP-L20 the level of accumulation of PGE$_1$ in the lesion site was much higher than that obtained with NP-DL20. As the latter shows low stability in serum, this accumulation is probably mediated by the EPR effect. However, the extent of accumulation of NP-L20 was not as evident as that observed in spinal injury sites.[32]

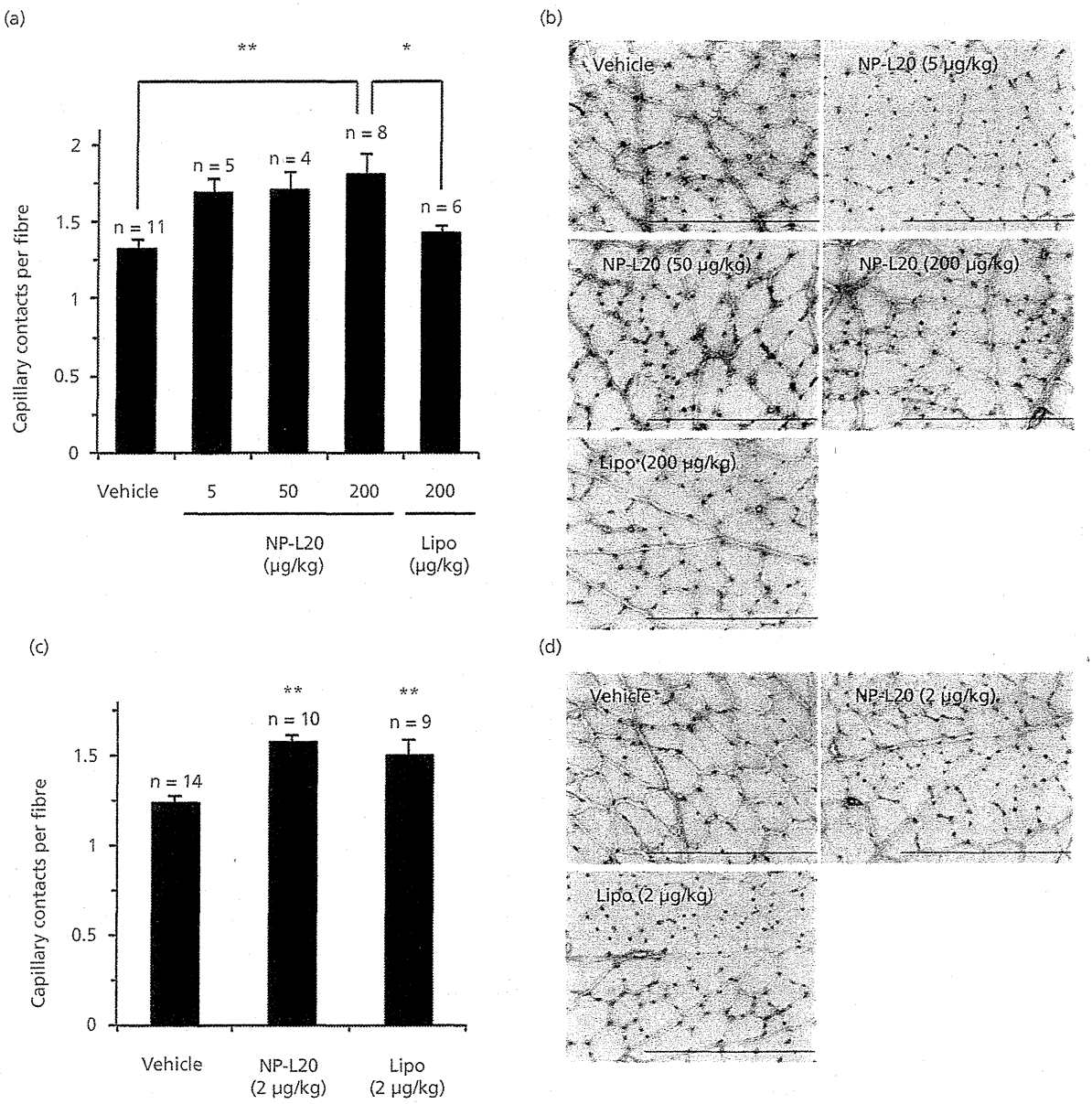

Figure 4 Effect of NP-L20, Lipo-PGE$_1$ or NP-DL20 on angiogenesis in the rat femoral artery ligation model. With respect to the results presented in Figures 2 or 3 (shown here in (a, b) and (c, d), respectively), one day after the last treadmill walking test, sections prepared from the white gastrocnemius muscle were subjected to immunohistochemical analysis with an antibody against CD31, as described in the Methods. Results were quantified, and data expressed as number of capillaries per muscle fibre (a, c). Values are presented as the mean ± S.E.M. $^{**}P < 0.01$, $^{*}P < 0.05$ (a, by the Tukey test; Vehicle, $n = 11$; NP-L20 5 μg/kg, $n = 5$; NP-L20 50 μg/kg, $n = 4$; NP-L20,200 μg/kg, $n = 8$; Lipo 200 μg/kg, $n = 6$; c, by the Tukey test; Vehicle, $n = 14$; NP-DL20 2 μg/kg, $n = 10$; Lipo 2 μg/kg, $n = 9$). Representative images of immunohistochemical analysis are shown (b, d). Scale bar, 300 μm.

We found that a single intravenous administration of NP-L20, but not of NP-DL20 or Lipo-PGE$_1$, improved the walking activity of femoral artery-ligated rats. Since repeated (daily) intravenous administration of NP-DL20 or Lipo-PGE$_1$ also improved walking activity, these results suggest that NP-L20 improves walking activity through the accumulation and sustained release of PGE$_1$.

It is known that tissue ischaemia induces angiogenesis (proliferation of muscle capillaries), which contributes to the improvement in blood supply around ischaemic

regions. We found here that angiogenesis in muscle around the ligated femoral artery was stimulated by a single intravenous administration of NP-L20. Angiogenesis was also observed in a similar manner in response to repeated (daily) administrations of NP-DL20 or Lipo-PGE$_1$. These results suggest that NP-L20 could stimulate angiogenesis in skeletal muscle through its accumulation and sustained release of PGE$_1$, and that this effect may be involved in the improvement of walking ability.

The remaining issue to be addressed concerns the dose of NP-L20 (200 μg/kg) required for the improvement of walking activity. The clinical dose of Lipo-PGE$_1$ is 10 μg/body weight/day and we found here that daily administration of 2 μg/kg Lipo-PGE$_1$ showed a tendency to improve walking ability. On the assumption that NP-L20 releases PGE$_1$ for 14 days (based on in-vitro data[20]), a single administration of NP-L20 of about 30 μg/kg would have been expected to show pharmacological activity. However, the results in this study revealed that 50 μg/kg NP-L20 did not improve walking ability clearly. The reason for this is not apparent at present, although we consider that the NP-L20 might be too stable and therefore the release of PGE$_1$ is too slow to maintain high concentrations of PGE$_1$ around the ligated femoral artery. On the other hand, we previously reported that Nano-PGE$_1$ (5 μg/kg) promoted the recovery of spinal injury-induced motor dysfunction.[32] This difference may be caused by the extensive accumulation of NP-L20 around injured spinal cord.

Conclusions

The findings of this study suggest that Nano-PGE$_1$ (NP-L20) improves the walking activity of femoral artery-ligated rats through the accumulation and sustained release of PGE$_1$.

Declarations

Conflict of interest

The Author(s) declare(s) that they have no conflicts of interest to disclose.

Funding

This work was supported by Grants-in-Aid for Scientific Research from the Ministry of Health, Labour, and Welfare of Japan, as well as the Japan Science and Technology Agency and Grants-in-Aid for Scientific Research from the Ministry of Education, Culture, Sports, Science and Technology, Japan.

References

1. Fujiwara T *et al.* Prevalence of asymptomatic arteriosclerosis obliterans and its relationship with risk factors in inhabitants of rural communities in Japan: Tanno-Sobetsu study. *Atherosclerosis* 2004; 177: 83–88.
2. Norgren L *et al.* Inter-Society Consensus for the Management of Peripheral Arterial Disease (TASC II). *J Vasc Surg* 2007; 45(Suppl. S): S5–67.
3. Shammas NW. Epidemiology, classification, and modifiable risk factors of peripheral arterial disease. *Vasc Health Risk Manag* 2007; 3: 229–234.
4. Caro J *et al.* The morbidity and mortality following a diagnosis of peripheral arterial disease: long-term follow-up of a large database. *BMC Cardiovasc Disord* 2005; 5: 14.
5. Rowlands TE, Donnelly R. Medical therapy for intermittent claudication. *Eur J Vasc Endovasc Surg* 2007; 34: 314–321.
6. Weiss C *et al.* Hemostasis and fibrinolysis in patients with intermittent claudication: effects of prostaglandin E1. *Prostaglandins Leukot Essent Fatty Acids* 2000; 63: 271–277.
7. Makino H *et al.* Increase in peripheral blood flow by intravenous administration of prostaglandin E1 in patients with peripheral arterial disease, accompanied by up-regulation of hepatocyte growth factor. *Hypertens Res* 2004; 27: 85–91.
8. Schror K, Hohlfeld T. Mechanisms of anti-ischemic action of prostaglandin E1 in peripheral arterial occlusive disease. *Vasa* 2004; 33: 119–124.
9. Bone RC *et al.* Randomized double-blind, multicenter study of prostaglandin E1 in patients with the adult respiratory distress syndrome. Prostaglandin E1 Study Group. *Chest* 1989; 96: 114–119.
10. Amendt K. PGE(1) and other prostaglandins in the treatment of intermittent claudication: a meta-analysis. *Angiology* 2005; 56: 409–415.
11. Ferreira SH, Vane JR. Prostaglandins: their disappearance from and release into the circulation. *Nature* 1967; 216: 868–873.
12. Golub M *et al.* Metabolism of prostaglandins A1 and E1 in man. *J Clin Invest* 1975; 56: 1404–1410.
13. Monkhouse DC *et al.* Kinetics of dehydration and isomerization of prostaglandins E 1 and E 2. *J Pharm Sci* 1973; 62: 576–580.
14. Mizushima Y *et al.* Prostaglandin E1 is more effective, when incorporated in lipid microspheres, for treatment of peripheral vascular diseases in man. *J Pharm Pharmacol* 1983; 35: 666–667.
15. Mizushima Y. Lipo-prostaglandin preparations. *Prostaglandins Leukot Essent Fatty Acids* 1991; 42: 1–6.
16. Mizushima Y. Lipid microspheres as novel drug carriers. *Drugs Exp Clin Res* 1985; 11: 595–600.
17. Mizushima Y *et al.* Distribution of lipid microspheres incorporating prostaglandin E1 to vascular lesions. *Prostaglandins Leukot Essent Fatty Acids* 1990; 41: 269–272.
18. Ruffolo AJ *et al.* Prostanoids for critical limb ischaemia. *Cochrane Database Syst Rev* 2010; (1)CD006544.

19. Igarashi R *et al.* A stable PGE1 prodrug for targeting therapy. *J Control Release* 1992; 20: 37–46.
20. Ishihara T *et al.* Prolonging the in vivo residence time of prostaglandin E(1) with biodegradable nanoparticles. *Pharm Res* 2008; 25: 1686–1695.
21. Maeda H *et al.* Tumor vascular permeability and the EPR effect in macromolecular therapeutics: a review. *J Control Release* 2000; 65: 271–284.
22. Gref R *et al.* Biodegradable long-circulating polymeric nanospheres. *Science* 1994; 263: 1600–1603.
23. Stolnik S *et al.* Surface modification of poly(lactide-co-glycolide) nanospheres by biodegradable poly (lactide)-poly(ethylene glycol) copolymers. *Pharm Res* 1994; 11: 1800–1808.
24. Ishihara T *et al.* Efficient encapsulation of a water-soluble corticosteroid in biodegradable nanoparticles. *Int J Pharm* 2009; 365: 200–205.
25. Yamaguchi T, Mizushima Y. Lipid microspheres for drug delivery from the pharmaceutical viewpoint. *Crit Rev Ther Drug Carrier Syst* 1994; 11: 215–229.
26. Ishiwata N *et al.* NT-702 (parogrelil hydrochloride, NM-702), a novel and potent phosphodiesterase inhibitor, improves reduced walking distance and lowered hindlimb plantar surface temperature in a rat experimental intermittent claudication model. *Life Sci* 2007; 81: 970–978.
27. Sasaki Y *et al.* K-134, a phosphodiesterase 3 inhibitor, improves gait disturbance and hindlimb blood flow impairment in rat peripheral artery disease models. *Eur J Pharmacol* 2012; 689: 132–138.
28. Ozumi K *et al.* Extracellular superoxide dismutase overexpression reduces cuff-induced arterial neointimal formation. *Atherosclerosis* 2005; 181: 55–62.
29. Cornachione A *et al.* Effects of eccentric and concentric training on capillarization and myosin heavy chain contents in rat skeletal muscles after hindlimb suspension. *Acta Histochem* 2011; 113: 277–282.
30. Dai S *et al.* Endothelial-specific expression of mitochondrial thioredoxin promotes ischemia-mediated arteriogenesis and angiogenesis. *Arterioscler Thromb Vasc Biol* 2009; 29: 495–502.
31. Ikenaga S *et al.* Autologous bone marrow implantation induced angiogenesis and improved deteriorated exercise capacity in a rat ischemic hindlimb model. *J Surg Res* 2001; 96: 277–283.
32. Takenaga M *et al.* Nano PGE1 promoted the recovery from spinal cord injury-induced motor dysfunction through its accumulation and sustained release. *J Control Release* 2010; 148: 249–254.

Tetrahedron
journal homepage: www.elsevier.com

Chemo-enzymatic enantioconvergent approach toward ethyl shikimate from ethyl 5-hydroxy-3,4-isopropylidenedioxycyclohex-1-enecarboxylate

Yasunobu Yamashita, Kengo Hanaya, Takeshi Sugai, Tohru Mizushima, Mitsuru Shoji*

Faculty of Pharmacy, Keio University, 1-5-30 Shibakoen, Minato-ku, Tokyo 105-8512, Japan

ARTICLE INFO

Article history:
Received
Received in revised form
Accepted
Available online

Keywords:
Ethyl shikimate
Enantioconvergent approach
Lipase
Kinetic resolution
Carbacycle

ABSTRACT

An enantioconvergent route for natural form of ethyl shikimate was achieved from Diels–Alder adduct of furan and acryloyl chloride. The key step was a highly enantioselective (E >500) and efficient acetylation of ethyl (3*R**,4*S**,5*S**)-5-hydroxy-3,4-isopropylidenedioxycyclohex-1-enecarboxylate, which had a diastereomeric relationship with ethyl shikimate, mediated by *B. cepacia* lipase (Amano PS-IM). Both of the resolved enantiomers were converted to natural form of ethyl shikimate by inversion at C-5 for the former and at C-3 and C-4 for the latter, respectively.

1. Introduction

Ethyl shikimate (**1**) is well-known intermediate for the synthesis of oseltamivir phosphate (Tamiflu®), which is a neuraminidase inhibitor used in the treatment of both Type A and B human influenza.[1] Shikimic acid (Scheme 1),[2] a starting material for the synthesis of oseltamivir phosphate, has been obtained from the extracts of Chinese star anis and is recently supplied by biosynthesis of engineered microorganism.[3] The production from fermented coffee pulp combined with another microbial transformation is also promising.[4] Synthetically, Diels–Alder reaction between furan and acrylic acid or its derivatives is a robust approach for the construction of cyclohexenecarboxylate framework in shikimic acid. The Diels–Alder reaction and subsequent diastereoselective transformations, however, gave "racemic" form of the polyoxygenated carbacycles. Pioneering works on enzyme-catalyzed kinetic resolution,[5] asymmetric Diels–Alder reaction,[6] and ring-closing metathesis[7] toward natural type of shikimic acid have been reported. Herein we describe an enantioconvergent approach to ethyl shikimate (**1**) by designing a readily accessible intermediate via lipase-mediated kinetic resolution of the cyclohexenol.

2. Results and discussion

In our synthetic plan as illustrated in Scheme 1, both **2** and **3** would be converted to natural form of ethyl shikimate (**1**) by regioselective inversion of stereochemistry at C-5 on **2** and at C-3 and C-4 on **3**, respectively. Optically active **2** and **3** would be obtained via lipase-mediated kinetic resolution of (±)-**4**, which would be produced by Diels–Alder reaction between furan and acryloyl chloride followed by β-elimination of bicycloester (±)-**5**.

Diels–Alder reaction between furan and acryloyl chloride[8] and subsequent quenching with ethanol (EtOH) gave a 1:1.4 mixture of *endo*-(±)-**6** and *exo*-(±)-**7** in 77% yield over two steps (Scheme 2). Although the *endo/exo* selectivity was low, these two adducts were converged on single diastereomer at a later stage. The next diastereoselective dihydroxylation catalyzed by $K_2OsO_2(OH)_4$ (1 mol%) provided a mixture of (±)-**8** and (±)-**9** quantitatively. In this dihydroxylation, higher loading of $K_2OsO_2(OH)_4$ caused the dihydroxylation from concave face. Protection of diol **8** and **9** as acetonide afforded a mixture of **10** and **11** in 96% yield over two steps. Subsequent β-elimination of **10** and **11** with lithium hexamethyldisilazide (LHMDS) in tetrahydrofuran (THF) at low temperature furnished (±)-**12** in 93% yield.

* Corresponding author. Tel.: +81-3-5400-2659; fax: +81-3-5400-2695; e-mail: shoji-mt@pha.keio.ac.jp

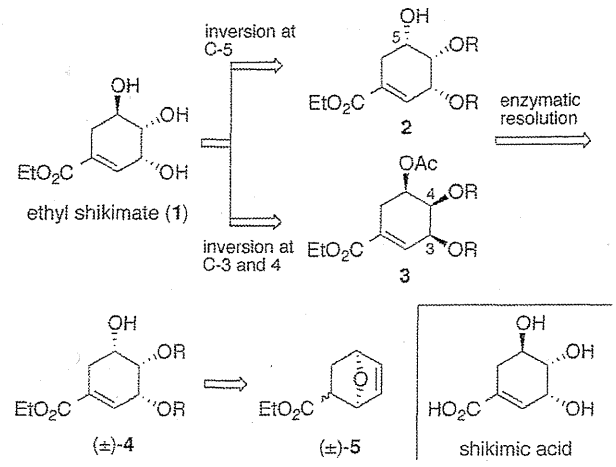

Scheme 1. Enantioconvergent retrosynthesis of **1**.

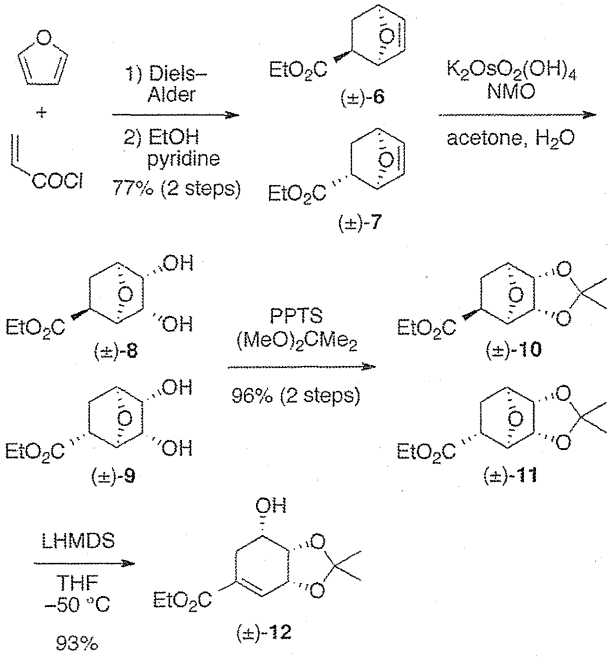

Scheme 2. Synthesis of (±)-**12** as a substrate for the enzymatic resolution.

Since the desired (±)-**12** was in hand, lipase-catalyzed acetylation was investigated with three commercially available enzymes such as *Candida rugosa* lipase (Meito OF), *Burkholderia cepacia* lipase (Amano PS-IM), and *Candida antarctica* lipase (Novozym 435) as shown in Scheme 3. The results are summarized in Table 1.

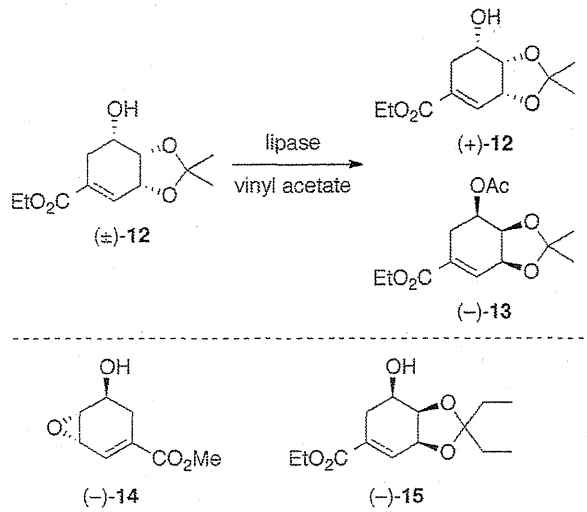

Scheme 3. Lipase-catalyzed resolution of racemic **12**.

With the former two enzymes, (−)-**12** was acetylated faster than (+)-**12** (entries 1 and 2) and the reactions proceeded with high enantioselectivities in both cases (E value[9] >500). The bulkier substituent was isopropylidenedioxy group in case of (−)-**12**,[10] whereas methoxycarbonyl group was larger in the "fast" enantiomer of structurally related substrate (−)-**14**.[8] Interestingly, *C. antarctica* lipase showed the opposite enantiomeric preference compared with the other lipases (entry 3). When bulkier substituent such as 3-pentylidenedioxy group was introduced in (±)-**15**, the reactivity of "fast" enantiomer decreased with the result of low enantioselectivity (E = 124) and incomplete conversion (entry 4). The acetylations with *B. cepacia* and *C. antarctica* lipases were almost no reaction.

Compared with Meito OF, Amano PS-IM was stable and reliable because it was immobilized to resin. Based on the result of entry 2 in Table 1, the scaled-up reaction was performed with 15 g of (±)-**12** to afford acetate (−)-**13** (8.3 g, 48.5% yield, 99.8% ee) and alcohol (+)-**12** (7.4 g, 49.3% yield, 98.0% ee). The ee of the latter could further be increased by recrystallization.

The next task was the transformation of "slow" enantiomer (+)-**12** into ethyl shikimate [(−)-**1**]. Immediately after the conversion of alcohol **12** into triflate **16**, inversion of stereochemistry at C-5 with KNO_2 in *N*,*N*-dimethylformamide (DMF) at room temperature provided (−)-**17** (75% over two steps, Scheme 4).[11] Mesylate and chloromethylsulfonate derived from **12** gave undesired aromatized byproduct because higher temperature for the inversion was required. The absolute configuration of **17** was determined to be (3*R*,4*S*,5*R*) by the comparison of its sign of optical rotation $[[\alpha]_D^{26}$ −33.0 (*c* 0.50, EtOAc)] with the reported value $[[\alpha]_D^{25}$ −31.0 (*c* 3.0, EtOAc)].[12]

Table 1. Lipase-catalyzed kinetic resolution of (±)-**12** and (±)-**15**.[a]

Entry	Substrate	Lipase	Time/h	Conv./%	E value[b]
1	(±)-**12**	*C. rugosa* (Meito OF)	4	50	>500[c]
2	(±)-**12**	*B. cepacia* (Amano PS-IM)	2	50	>500[c]
3	(±)-**12**	*C. antarctica* B (Novozym 435)	38	45.8	71[d]
4	(±)-**15**	*C. rugosa* (Meito OF)	16	44.7	124[c]

[a]For detailed conditions, see experimental section.

[b]Calculated according to ref. 9.

[c]The (−)-enantiomer reacted faster.

[d]The (+)-enantiomer reacted faster.

Removal of acetonide of **17** worked well by the treatment with Dowex 50W-X8 (H^+ form) in EtOH to accomplish the synthesis of natural form of ethyl shikimate [(–)-**1**] in 78% yield. Since triol **1** was soluble in aqueous phase, deprotection under acidic condition such as pyridinium *p*-toluenesulfonate in methanol followed by aqueous workup resulted in a low yield (54%).

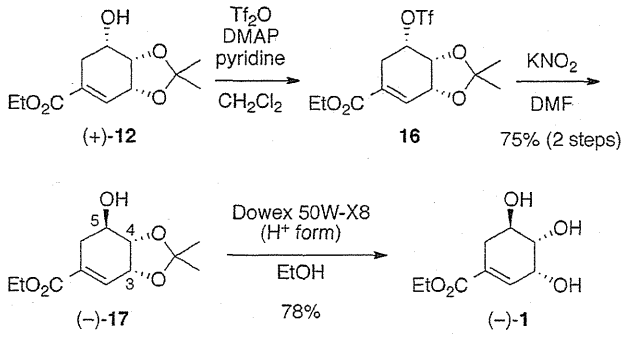

Scheme 4. Synthesis of natural form of ethyl shikimate (**1**) from (+)-**12**.

Toward the enantioconvergent approach, the next task was the synthesis of ethyl shikimate (**1**) from (–)-**13**, which was the "fast" isomer of the lipase-catalyzed kinetic resolution. Our first attempt was the removal of acetonide under acidic condition with Brønsted acids such as Dowex 50W-X8 (H^+ form) or PPTS in alcoholic solvents. Those conditions, however, caused solvolysis of acetyl group along with the removal of acetonide to give the triol (*ca.* 30%) with the equal amount of desired **18**. The yield of this step was improved by Lewis acidic condition using $FeCl_3 \cdot 6H_2O$ to afford **18** in 87% yield (Scheme 5).

Attempts for the simultaneous inversion of the stereochemistry at C-3 and C-4 of **18** via the corresponding dimesylate, bischloromethylsulfonate, and ditriflate, resulted in the complex mixture of structurally undefined products. Thus, a stepwise and successive route was employed. At first, diol at C-3 and C-4 was activated as cyclic sulfite **19**. Acetate was introduced to C-3 allylic position by the treatment of cesium acetate to give inverted acetate **20**. Since the acidity of H-3 was high because of allylic position and electron-withdrawing acetyl group, allylic acetate **20** easily decomposed. Thus, diacetate **20** was transformed to ethyl shikimate (**1**) as soon as possible without purification. The hydroxy group at C-4 position was triflated, and the resulting triflate **21** was immediately treated with KNO_2 in DMF to provide **22**. Since deprotection of diacetate **22** by *C. antarctica* lipase (Novozym 435) required long reaction time to cause decomposition, final removal of the two acetyl groups was performed under acidic condition to furnish ethyl shikimate [(–)-**1**] in 7% yield over five steps.

3. Conclusion

A "diastereomeric substrate" (±)-**12** for lipase-catalyzed kinetic resolution was prepared and reliable (E >500, conv. = 50%) resolution condition was elaborated with the use of *B. cepacia* lipase (Amano PS-IM). Both of the resolved enantiomers were converted to natural form of ethyl shikimate [(–)-**1**] with high enantiomeric excess by way of regioselective inversion of the stereochemistry. The enantioconvergent synthesis of (–)-**1** was achieved in 59% yield over three steps and in 6% yield over six steps from (+)-**12** and (–)-**13**, respectively.

4. Experimental section

4.1. General methods

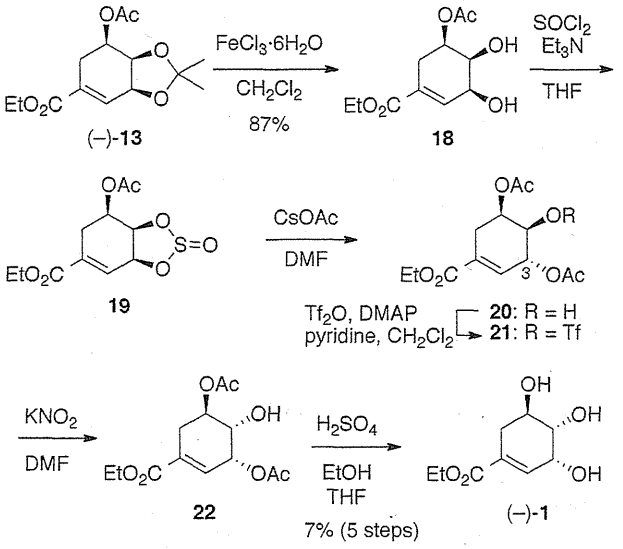

Scheme 5. Synthesis of ethyl shikimate (**1**) from (–)-**13**.

IR spectra were measured as thin films for oil or ATR for solid. ^1H and ^{13}C NMR spectra were measured in $CDCl_3$ at 400 and 100 MHz, respectively. HRMS analysis was recorded on a FAB-MS mass spectrometer. Column chromatography was performed on silica gel.

4.2. Ethyl (1R,2S*,5S*)-2,5-epoxycyclohex-3-enecarboxylate (6, endo isomer) and (1R*,2R*,5R*)-2,5-epoxycyclohex-3-enecarboxylate (7, exo isomer).*

To furan (32 mL, 440 mmol) was added acryloyl chloride (9 mL, 110 mmol) and the mixture was stirred for 72 h at room temperature. After evaporation of the excess reagents, to the residue were added pyridine (26 mL) and EtOH (30 mL) and the mixture was stirred for 1 h at room temperature. The reaction mixture was cooled to 0 °C, and the reaction was quenched with water. Organic materials were extracted with EtOAc. The combined extract was washed with 2 M HCl aq. solution, saturated $NaHCO_3$ aq. solution and brine, dried over Na_2SO_4, and concentrated *in vacuo*. The residue was purified by silica gel column chromatography (100 g). Elution with hexane-EtOAc (2:1) afforded a mixture of (±)-**6** (*endo*) and (±)-**7** (*exo*) as a pale yellow oil (14.2 g, 77%, *endo*:*exo* = 1:1.4). IR (neat) 2981, 1722, 1450, 1369, 1317, 1184, 1045, 1020, 906, 875, 703 cm^{-1}; ^1H NMR ($CDCl_3$) δ 6.42 (d, J = 5.9 Hz, 1H, *endo*), 6.37 (d, J = 5.8 Hz, 1H, *exo*), 6.33 (d, J = 5.8 Hz, 1H, *exo*), 6.21 (d, J = 5.9 Hz, 1H, *endo*), 5.17 (s, 1H, *exo*), 5.14 (d, J = 5.5 Hz, 1H, *endo*), 5.05 (d, J = 4.3 Hz, 1H, *exo*), 5.00 (d, J = 4.7 Hz, 1H, *endo*), 4.16 (q, J = 7.2 Hz, 2H, *exo*), 4.08 (q, J = 7.1 Hz, 2H, *endo*), 3.08 (dt, J = 8.8, 3.9 Hz, 1H, *endo*), 2.40 (dd, J = 8.7, 4.0 Hz, 1H, *exo*), 2.14 (ddd, J = 11.5, 8.7, 4.3 Hz, 1H, *exo*), 2.07 (ddd, J = 11.6, 8.8, 4.7 Hz, 1H, *endo*), 1.55 (dd, J = 11.6, 3.9 Hz, 1H, *endo*), 1.54 (dd, J = 11.5, 4.0, 1H, *exo*), 1.25 (t, J = 7.2 Hz, 3H, *exo*), 1.22 (t, J = 7.1 Hz, 3H, *endo*); ^{13}C NMR ($CDCl_3$) δ 174.3, 172.7, 137.7, 135.3 (2C), 133.1, 81.5, 79.6, 79.4, 78.6, 61.5, 61.4, 43.5, 43.4, 29.6, 29.1, 14.8 (2C).

4.3. Ethyl (1R,2R*,3S*,4R*,5S*)-2,5-epoxy-3,4-dihydroxycyclohexanecarboxylate (8, endo isomer) and (1R*,2S*,3R*,4S*,5R*)-2,5-epoxy-3,4-dihydroxycyclohexanecarboxylate (9, exo isomer).*

To a solution of the mixture of (±)-**6** and (±)-**7** as above (14.2 g, 84 mmol) in acetone (200 mL) and water (100 mL) were added *N*-methylmorpholine *N*-oxide (50% in water, 23.3 mL, 120 mmol) and $K_2OsO_2(OH)_4$ (255 mg, 0.84 mmol), and the mixture

was stirred for 8 h at room temperature. The reaction was quenched with saturated $Na_2S_2O_3$ aq. solution and organic materials were extracted with EtOAc three times. The combined extract was washed with brine, dried over Na_2SO_4 and concentrated *in vacuo*. The residue was purified by silica gel column chromatography (150 g). Elution with hexane-EtOAc (1:1) afforded a mixture of (±)-**8** (*endo*) and (±)-**9** (*exo*) as a yellow solid (16.9 g, 99%, *endo*:*exo* = 1:1.4). A small portion was separated by preparative TLC [developed with hexane-EtOAc (1:2)] to afford analytically pure samples of (±)-**8** and (±)-**9** as colorless solids respectively. (±)-**8**: IR (neat) 3371, 3305, 2989, 2958, 1720, 1450, 1187, 1068, 995, 910 cm^{-1}; ^1H NMR ($CDCl_3$) δ 4,46 (d, J = 5.9 Hz, 1H), 4.36 (d, J = 5.7 Hz, 1H), 4.13 (q, J = 7.1 Hz, 2H), 3.92 (d, J = 6.0 Hz, 1H), 3.89 (d, J = 6.0 Hz, 1H), 3.33 (bs, 2H), 2.92 (dt, J = 11.4, 5.9 Hz, 1H), 1.88 (ddd, J = 12.7, 11.4, 5.7 Hz, 1H), 1.75 (dd, J = 12.7, 5.9 Hz, 1H), 1.24 (t, J = 7.1 Hz, 3H); ^{13}C NMR ($CDCl_3$) δ 171.7, 83.4, 82.80, 74.8, 72.0, 61.3, 44.0, 28.4, 14.3; mp 83.5-84.0 °C. Anal. Calcd for $C_9H_{14}O_5$: C, 53.46; H, 6.98; Found: C, 53.36; H, 6.95. (±)-**9**: IR (neat) 3386, 3317, 2981, 2950, 1720, 1446, 1045, 1002, 898, 771, cm^{-1}; ^1H NMR ($CDCl_3$) δ 4.57 (s, 1H), 4.40 (d, J = 5.7 Hz, 1H), 4.12 (q, J = 7.1 Hz, 2H), 3.86 (d, J = 5.9 Hz, 1H), 3.82 (d, J = 5.9 Hz, 1H), 3.50 (bs, 2H), 2.47 (dd, J = 9.2, 4.9 Hz, 1H), 2.04 (ddd, J = 12.9, 5.7, 4.9 Hz, 1H), 1.58 (dd, J = 12.9, 9.2 Hz, 1H), 1.23 (t, J = 7.1 Hz, 3H); ^{13}C NMR ($CDCl_3$) δ 172.9, 84.5, 82.0, 74.4, 74.3, 61.4, 43.1, 29.0, 14.3; mp 86.5-87.1 °C; Anal. Calcd for $C_9H_{14}O_5$: C, 53.46; H, 6.98; Found: C, 53.50; H, 6.98.

4.4. Ethyl (1R,2R*,3S*,4R*,5S*)-2,5-epoxy-3,4-isopropylidenedioxycyclohexanecarboxylate (**10**, endo isomer) and (1R*,2S*,3R*,4S*,5R*)-2,5-epoxy-3,4-isopropylidenedioxycyclohexanecarboxylate (**11**, exo isomer).*

To a solution of the mixture of (±)-**8** and (±)-**9** as above (16.9 g, 84 mmol) in acetone (200 mL) were added 2,2-dimethoxypropane (36 mL, 256 mmol) and pyridinium *p*-toluenesulfonate (4.0 g, 15 mmol) and the mixture was stirred for 36 h at room temperature. The reaction was quenched with saturated $NaHCO_3$ aq. solution and organic materials were extracted with EtOAc. The combined extract was washed with brine, dried over Na_2SO_4, and concentrated *in vacuo*. The residue was purified by silica gel column chromatography (200 g). Elution with hexane-EtOAc (3:1) afforded a mixture of (±)-**10** (*endo*) and (±)-**11** (*exo*) as a yellow solid (19.5 g, 96%, *endo*:*exo* = 1:1.4). A small portion was separated by preparative TLC [developed with hexane-EtOAc (2:1)] to afford analytical pure samples of (±)-**10** and (±)-**11** as colorless solids respectively. (±)-**10**: IR (neat) 2981, 2939, 1720, 1373, 1195, 1160, 1049, 1002, 867 cm^{-1}; ^1H NMR ($CDCl_3$) δ 4.53 (d, J = 5.8 Hz, 1H), 4.42 (d, J = 6.0 Hz, 1H), 4.26 (s, 2H), 4.15 (q, J = 7.2 Hz, 2H), 2.94 (dt, J = 11.2, 5.8 Hz, 1H), 1.89 (ddd, J = 12.9, 11.2, 6.0 Hz, 1H), 1.70 (dd, J = 12.9, 5.8 Hz, 1H), 1.45 (s, 3H), 1.27 (t, J = 7.2 Hz, 3H), 1.25 (s, 3H); ^{13}C NMR ($CDCl_3$) δ 171.7, 111.1, 82.2, 80.2, 79.7, 79.5, 61.3, 43.3, 27.2, 25.9, 25.0, 14.3; mp 46.1-46.7 °C; HRMS (FAB-MS): Calcd. for $C_{12}H_{19}O_5$: $[M+H]^+$: 243.1232; Found: m/z = 243.1237. (±)-**11**: IR (neat) 2981, 2962, 1727, 1268, 1203, 1153, 1072, 1033, 1002, 856 cm^{-1}; ^1H NMR ($CDCl_3$) δ 4.65 (s, 1H), 4.46 (d, J = 5.8 Hz, 1H), 4.22 (q, J = 7.0 Hz, 2H), 4.15 (d, J = 5.7 Hz, 1H), 4.13 (d, J = 5.7 Hz, 1H), 2.37 (dd, J = 9.2, 4.9 Hz, 1H), 2.11 (ddd, J = 12.9, 5.8, 4.9 Hz, 1H), 1.52 (s, 3H), 1.48 (dd, J = 12.9, 9.0 Hz, 1H), 1.45 (s, 3H), 1.24 (t, J = 7.0 Hz, 3H); ^{13}C NMR ($CDCl_3$) δ 172.5, 111.8, 82.3, 82.1, 82.0, 78.7, 61.2, 42.1, 27.7, 25.9, 25.2, 14.2; mp 48.5-49.2 °C; Anal. Calcd for $C_{12}H_{18}O_5$: C, 59.49; H, 7.49; Found: C, 59.50; H, 7.43.

4.5. Ethyl (3R,4S*,5S*)-5-hydroxy-3,4-isopropylidenedioxycyclohex-1-enecarboxylate (**12**).*

To a solution of hexamethyldisilazane (25 mL, 96 mmol) in THF (400 mL) was added *n*-BuLi solution (1.57 M in hexane, 72 mL, 104 mmol) dropwise at 0 °C and the mixture was stirred for 10 min at that temperature. To the mixture was added a solution of the mixture of (±)-**10** and (±)-**11** as above (19.5 g, 80 mmol) in THF (80 mL) dropwise at –50 °C and the mixture was stirred for 30 min at that temperature. The reaction was quenched with saturated NH_4Cl aq. solution and organic materials were extracted with EtOAc. The combined extract was washed with brine, dried over Na_2SO_4, and concentrated *in vacuo*. The residue was purified by silica gel column chromatography (200 g). Elution with hexane-EtOAc (2:1) afforded (±)-**12** as a colorless solid (18.1 g, 93%). IR (neat) 3440, 2985, 2935, 2912, 1708, 1365, 1226, 1095, 1049, 909, 852, 732 cm^{-1}; ^1H NMR ($CDCl_3$) δ 6.77 (s, 1H), 4.70 (m, 1H), 4.39 (dd, J = 5.9, 2.7 Hz, 1H), 4.19 (q, J = 7.0 Hz, 2H), 3.93 (ddd, J = 8.2, 4.5, 2.7 Hz, 1H), 2.62 (dd, J = 16.6, 4.9 Hz, 1H), 2.49 (dd, J = 16.7, 8.2 Hz, 1H), 1.39 (s, 3H), 1.37 (s, 3H), 1.28 (t, J = 7.0 Hz, 3H); ^{13}C NMR ($CDCl_3$) δ 166.8, 135.0, 130.0, 110.5, 76.0, 73.4, 67.5, 61.5, 28.2, 27.9, 26.5, 14.6; mp 46.1-47.1 °C; Anal. Calcd for $C_{12}H_{18}O_5$: C, 59.49; H, 7.49; Found: C, 59.48; H, 7.43.

*4.6. Lipase-catalyzed acetylation of (±)-**12** and (±)-**15**.*

To a mixture of alcohol (±)-**12** (15 g, 62 mmol) in vinyl acetate (100 mL) was added *Burkholderia cepacia* lipase (Amano PS-IM, 5 g) and the mixture was stirred for 8 h at room temperature. The lipase was filtered off and the filtrate was concentrated *in vacuo*. The residue was purified by silica gel column chromatography (200 g). Elution with hexane-EtOAc (2:1) firstly afforded acetate (–)-**13** as a colorless solid (8.3 g, 48.5%), and secondly, alcohol (+)-**12** (7.4 g, 49.3%). (–)-**13**: HPLC analysis [column, Daicel Chiralcel AY-3, 0.46 cm × 25 cm; hexane-isopropyl alcohol (30:1); flow late 0.5 mL min^{-1}; detected at 210 nm]: t_R (min) = 21.8 [(–)-**13**, 99.9%], 23.9 [(+)-**13**, 0.1%]; IR (neat) 2987, 1733, 1702, 1373, 1214, 1064, 1039, 950, 862 cm^{-1}; ^1H NMR ($CDCl_3$) δ 6.76 (s, 1H), 5.06 (ddd, J = 7.6, 5.5, 2.1 Hz, 1H), 4.75 (d, J = 4.9 Hz, 1H), 4.41 (dd, J = 5.5, 2.1 Hz, 1H), 4.19 (q, J = 7.1, 2H), 2.67 (dd, J = 16.4, 5.5 Hz, 1H), 2.49 (dd, J = 16.4, 7.6 Hz, 1H), 2.11 (s, 3H), 1.38 (s, 3H), 1.35 (s, 3H), 1.27 (t, J = 7.1 Hz, 3H); ^{13}C NMR ($CDCl_3$) δ 171.2, 166.7, 135.6, 129.7, 111.4, 74.4, 74.3, 69.8, 61.8, 28.4, 27.3, 24.9, 21.9, 14.9; $[\alpha]_D^{26}$ –37.0 (*c* 1.00, MeOH); mp 71.1-71.5 °C; Anal. Calcd for $C_{14}H_{20}O_6$: C, 59.14; H, 7.06; Found: C, 59.20; H, 7.07. (+)-**12**: HPLC analysis [column, Daicel Chiralcel AY-3, 0.46 cm × 25 cm; hexane-isopropyl alcohol (30:1); flow late 0.5 mL min^{-1}; detected at 210 nm]: t_R (min) = 79.6 [(–)-**12**, 1.0%], 81.3 [(+)-**12**, 99.0%]; $[\alpha]_D^{26}$ +61.4 (*c* 0.60, MeOH). Its ^1H NMR spectrum was in good accordance with that of racemic sample.

To a mixture of alcohol (±)-**12** (10 mg, 0.041 mmol) in vinyl acetate (1 mL) was added *Candida rugosa* lipase (Meito OF, 10 mg) and the mixture was stirred for 4 h at room temperature. In the similar workup and separation as describe for *B. cepacia* lipase-catalyzed resolution, (–)-**13** (5.4 mg, 49.4%) and (+)-**12** (4.9 mg, 49.0%) were obtained. (+)-**12**: under the same conditions as above: t_R (min) = 79.6 [(–)-**12**, 0.1%], 81.3 [(+)-**12**, 99.9%]. (–)-**13**: HPLC under the same conditions as above: t_R (min) = 21.8 [(–)-**13**, 99.5%], 23.9 [(+)-**13**, 0.5%].

The reaction (38 h), workup, and purification with *C. antarctica lipase* B (Novozym 435) was carried out in a similar manner. From (±)-**12** (10 mg, 0.041 mmol), (+)-**13** (5.1 mg, 47.2%) and (–)-**12** (4.9 mg, 49.0%) were obtained. (–)-**12**: HPLC under the same conditions: t_R (min) = 79.6 [(–)-**12**, 85.8%],